Copyright Warning & Restrictions

The copyright law of the United States (Title 17, United States Code) governs the making of photocopies or other reproductions of copyrighted material.

Under certain conditions specified in the law, libraries and archives are authorized to furnish a photocopy or other reproduction. One of these specified conditions is that the photocopy or reproduction is not to be "used for any purpose other than private study, scholarship, or research." If a, user makes a request for, or later uses, a photocopy or reproduction for purposes in excess of "fair use" that user may be liable for copyright infringement,

This institution reserves the right to refuse to accept a copying order if, in its judgment, fulfillment of the order would involve violation of copyright law.

Please Note: The author retains the copyright while the New Jersey Institute of Technology reserves the right to distribute this thesis or dissertation

Printing note: If you do not wish to print this page, then select "Pages from: first page # to: last page #" on the print dialog screen

ABSTRACT

Measurement of Heart Rate Variability
Using Correlation Dimension and Entropy

by
Su Zhang

Heart rate variability regulation is controlled by the autonomic nervous system. Disorders of the autonomic nervous system may cause the loss of heart rate variability. Two new approaches, correlation dimension and entropy, based on ideas from nonlinear dynamics, have been applied to studying heart rate variability. The correlation dimension measures the extent of correlation between the data points. The entropy measures the amount of information needed to specify the state of a system. The interbeat interval signal (IBI) from eighteen subjects (nine normal controls and nine patients with Chronic Fatigue Syndrome (CFS)) have been analyzed and compared. The results show that the CFS patients have higher correlation dimension and lower entropy than normal subjects, which indicates that the heart rate variability is reduced for these patients. This suggests that there may be an autonomic nervous system imbalance in CFS patients.

MEASUREMENT OF HEART RATE VARIABILITY USING CORRELATION DIMENSION AND ENTROPY

by
Su Zhang

A Thesis
Submitted to the Faculty of
New Jersey Institute of Technology
in Partial Fulfillment of the requirements for the Degree of
Master of Science in Electrical Engineering

Department of Electrical and Computer Engineering

January 1994

APPROVAL PAGE

MEASUREMENT OF HEART RATE VARIABILITY USING CORRELATION DIMENSION AND ENTROPY

Su Zhang

Dr. Stanley S. Reisman, Thesis Advisor (Date)
Professor of Electrical and Computer Engineering, NJIT

Dr. Walter N. Tapp, Committee Member (Date)
Professor of Neurosciences, UMDNJ

Dr. Peter Engler, Committee Member (Date)
Professor of Electrical and Computer Engineering, NJIT

BIOGRAPHICAL SKETCH

Author: Su Zhang

Degree: Master of Science in Electrical Engineering

Date: January 1994

Undergraduate and Graduate Education:

- Master of Science in Electrical Engineering,
  New Jersey Institute of Technology, Newark, NJ, 1994

- Associate Bachelor of Science in Electrical Engineering
  Jiangsu TV and Radio University, Nanjing, China, 1983

- Bachelor of Science in Medicine
  Nanjing Medical College, Nanjing, China, 1976

Major: Electrical Engineering

Presentations and Publications:

Zhang, S., S.Reisman., W.Tapp., and Z.Zhang. 1992. "Correlation Dimension on Heart Rate Variability." 19th IEEE Northeast Bioengineering Conference. Newark, March, 1993.

ACKNOWLEDGMENT

The author would like to thank the following people for their efforts and support. The author wishes to express her sincere gratitude to her advisor, Dr. Stanley S. Reisman, for his guidance, encouragement and support through out this research. She would also like to thank Dr. Walter Tapp for his guidance. Special thanks to Dr. Peter Engler for serving as a member of the committee.

TABLE OF CONTENTS

Chapter **Page**

LIST OF TABLES

LIST OF FIGURES

Figure **Page**

CHAPTER 1

INTRODUCTION

1.1 Electrical Activity of the Heart

The synchronized mechanical activity of the heart depends on the propagation of electrical excitation waves, which trigger the complex sequence of biochemical processes involved in the contraction of the individual heart cells. Contraction of cardiac muscle, like that of other muscle types, is triggered by depolarization of the plasma membrane. About one percent of cardiac muscle cells, like certain forms of smooth muscle, are autorhythmic; i.e., they are capable of autonomous rhythmical self-excitation. Such a property, known as automaticity, occurs normally in the cells of the sinoatrial node, which is the region responsible for the initiation of each normal heartbeat. From the SA node, the pacemaker of the heart, the action potential spreads throughout both atria, reaching the AV node. The bundle of His, a conducting link between atria and ventricles, then carries the potential to the ventricles, causing the ventricles to contract. An ECG occurs during this process. Figure 1.1 illustrates a typical normal ECG. The first wave, P, represents atrial depolarization. The second complex, QRS, occurring approximately 0.1 to 0.2s later, represents ventricular depolarization and atrial repolarization. The final wave,T, represents ventricular repolarization.

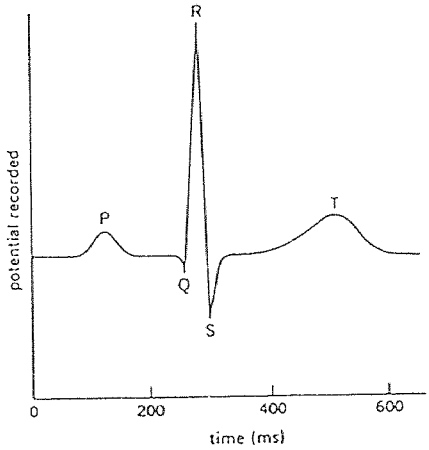

Figure 1.1 Typical electrocardiogram. P, atrial depolarization; QRS, ventricular depolarization; T, ventricular repolarization.

1.2 Current Research in Heart Rate Variability

If one listens to the heart through a stethoscope or feels the pulse at the wrist, the rhythm of the heart seems to be regular. For an individual at rest the pulse strength and the interval between heartbeats seem roughly constant. For this reason cardiologists routinely describe the normal heart rate as regular sinus rhythm. The traditional view of normal sinus rhythm as highly regular or periodic is contradicted by more careful analysis which reveals that healthy individuals have heart rates that fluctuate considerably even at rest. In healthy, young adults the heart rate, which averages about 60 beats per minute, may change as much as 20 beats per minute every few heartbeats. In the course of a day the heart rate may vary from 40 to 180 beats per minute[1].

Heart rate variability regulation is a mechanism controlled by the sympathetic and parasympathetic nervous systems. Sympathetic input generally increases heart rate while parasympathetic input decreases it. Furthermore, changes

in heart rate often reflect the reciprocal action of the sympathetic and parasympathetic systems. These spontaneous fluctuations in heart rate are normally considered a healthy sign. The wide variations in heart rate are commonly seen in healthy individuals. By contrast, a number of physiologic and disease states produce alterations in autonomic function which reduce the variability in heart rate.Recent research discovered that the pattern of heartbeats of patients with diabetes, multiple sclerosis, and fetal distress often became less variable than in normal people[1]. Therefore, irregularity and unpredictability are important features of health. On the other hand, decreased variability and accentuated periodicities are associated with disease. Therefore, in recent years the possibility of quantifying the heart rate variability has aroused a growing interest. The variability in heart rate has been used to study the function of the cardiovascular control system.

The measurement of heart rate variability involves taking the difference in time between successive R waves, which generates an interbeat interval (IBI) signal. First, the ECG signal is preprocessed to remove noise interference, and the variability is then measured from the R-R intervals by one of the conventional QRS detectors that defines the position of each QRS complex. A variety of methods have been proposed to analyze this signal,such as spectrum analysis, complex demodulation, standard deviation, autoregressive analysis and phase response curve methods[2][3][4].

A. Spectral Analysis

The most prominent technique used to analyze heart rate variability is spectrumanalysis. First, the R-R interval series must be interpolated to form an

equidistant time series. Then, taking the Fourier transform of the time series produces the heartbeat interval spectrum.

The basic proposition behind spectral analysis is that in human beings both divisions of the autonomic nervous system influence heart rate variability in a frequency-dependent way. Usually three major, identifiable peaks are distinguished in the power spectrum of interbeat interval variability(Figure 1.2)[2].

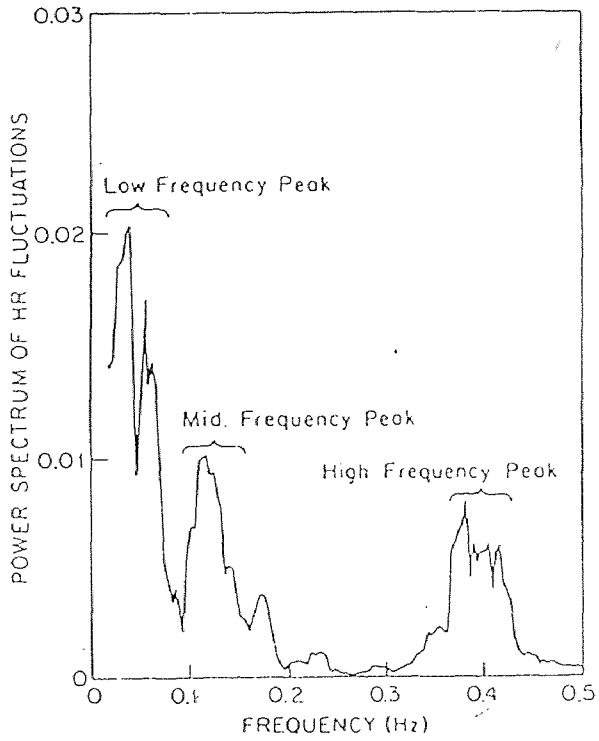

Figure 1.2 Power spectrum of instantaneous heart rate fluctuation featuring three peaks

The best-known and best-defined peak is respiration related, determined as the heart rate spectral power at the respiratory frequency(high frequency band, HF≈0.25 - 0.4Hz). It is purely parasympathetic in origin. The other well-understood peak occurs at frequencies lower than 0.05 Hz (low-frequency band, LF, 0.01 - 0.05Hz). It is mediated by both the sympathetic and parasympathetic systems. The

third peak, in the region of 0.1 --0.15Hz(middle-frequency band, MF), is associated with the frequency response of the baroreceptor reflex reflecting vagal activity.

B.Complex Demodulation

Power spectrum analysis only shows the "average of the spectrum over the entire length of the time series". However, autonomic regulation of the cardiovascular system can change rapidly in response to physical or psychological demands.

Complex demodulation is able to provide the time-local descriptions of heart rate variability necessary to characterize such changing autonomic regulation. The use of complex demodulation enables us to examine autonomic contributions to heart rate regulation in conditioning and a variety of other physiological and environmental conditions where autonomic input can be expected to change rapidly. Complex demodulation is a local version of harmonic analysis that enables us to describe the amplitude and phase of particular frequency components of a time series as functions of time. Consequently, complex demodulation can be used to study local changes of a signal over time.

Drs. Shin, Tapp and Reisman have succeeded in analyzing the data from dogs by complex demodulation during classical conditioning procedures which caused different changes in the autonomic regulation of heart rate[3]. Two significant peaks in the heart rate variability spectrum were examined by this technique. The amplitude of the peak at the respiration frequency showed parasympathetic changes, while the amplitude of the low frequency peak showed both sympathetic and parasympathetic effects. Complex demodulation results at these frequencies clearly showed the activities of both branches of the autonomic nervous system in

regulating heart rate.

C. Standard Deviation

Dr. Martin and others have analyzed data from patients who died suddenly during ambulatory monitoring by measuring the standard deviation of heart interbeat intervals[4]. Comparisons were made with heart rate variability findings in twenty normal subjects. The standard deviation of R-R intervals was significantly lower in the patients who died suddenly than in the normal subjects.

D. Phase Response Curve

Mr.Zhang, Drs. Reisman and Tapp[5] proposed a new approach to study the heart rate interaction with the respiration cycle. In the study, heart rate is treated as a system of homogeneous, self-sustained oscillators perturbed by respiration. Because respiration perturbs heart rate through the autonomic nervous system, the study examined this relationship producing a better understanding of the autonomic nervous system.

A phase respones curve can be constructed to predict the entrainment behavior of heart rate interacting with respiration. Their study shows that a large difference can be observed between normal and abnormal subjects.

1.3 Nonlinear Dynamic Study in Heart Rate Variability

The assessment of heart rate variation has been characterized classically by linear approaches such as autocorrelation histograms, spectral analysis and mean and variance measures. However, linear procedures are less useful for adequately assessing the time-dependent characteristics of cardiac variability because

variability seldom follows assumptions of stationarity upon which linear assessment techniques are based.

In recent years clinical cardiology offered many examples of nonlinear dynamic behavior which includes variability , sustained and complex oscillations, abrupt transitions, alternans and hysteresis. For example, different types of electrical and mechanical alternans -- where some variable alternates in value on a beat-to-beat basis, are well-described in life-threatening cardiac pathologies. ST segment alternans indicates severe ischemia and often heralds the sudden onset of ventricular fibrillation in both experimental and clinical conditions. Alternation in the strength of each heartbeat is a sign of severe ventricular dysfunction. Pericardial effusion with tamponade may lead to periodic swinging of the heart with consequent alternation of the entire ECG vector(electrical alternans)[6].

A detailed understanding of the dynamics of such systems must necessarily be carried out in the context of the mathematics of nonlinear systems. The complexity and nonlinearity make this nonlinear system inaccessible to conventional linear techniques. Recently, nonlinear dynamic (chaos theory) has provided a number of new statistical tools which have been applied to the analysis of biomedical systems, independent of traditional measures based on mean, variance, or Fourier Spectrum. The most widely used techniques derived from the theory of nonlinear dynamical systems are fractal dimension, entropy and Lyapunov exponents. The algorithms for fractal dimension and entropy are relatively easy to apply to a time series. They are statistics which, unlike the spectrum, are sensitive to nonlinear correlation in a time series.

The fractal dimension describes the dimension of the attractor of a dynamical system. It indicates the number of degrees of freedom in the dynamic system. The dimension of the attractor is an important feature in chaos, and by extension, the "dimension" of a time series is considered an important chaotic statistic. For a deterministic system the dimension is often interpreted as the number of dynamic variables in the difference or differential equations needed to construct a dynamical system that will reproduce the measured signal[7].

Another way to quantify complexity is by entropy, which deals with the amount of information needed to predict the future state of the system. It measures how much information is generated by a time series, e.g. the extent to which the future of the time series can be predicted by the past. More complex dynamics are represented as a large entropy, and random noise is maximally complex[8].

Dr.Theiler and others[9] describe a new statistical approach for identifying nonlinearity in time series. This is of particular interest to forecasters, who would like to know whether a given time series contains the kind of nonlinear structure that might be exploited by a nonlinear prediction algorithm. The method first specifies some linear process as a null hypothesis, then generates surrogate data sets which are consistent with this null hypothesis, and finally computes a discriminating statistic for the original and for each of the surrogate data sets. If the value computed for the original data is significantly different from the ensemble of values computed for the surrogate data, then the null hypothesis is rejected and nonlinearity is detected.

1.4 The Present Research

Recently, a general qualitative hypothesis of variability and pathology has been proposed: the dynamics of the healthy physiological control system produce an apparently irregular and highly complex type of variability, whereas disease is often associated with more regularity and less complexity[1].

Based on this idea, we used several techniques to study dynamics activity of heart rate variability in both healthy people and patients with Chronic Fatigue Syndrome(CFS). CFS is an illness of unknown origin whose primary symptom is extreme, devastating fatigue, compounded by mild fever, sore throat, painful or palpable lymph nodes, unexplained muscle weakness and/or discomfort, headaches, cognitive impairment and sleep disturbance. CFS differs from the more typical feeling of fatigue; it is a debilitating disorder that interferes with a person's ability to participate in the activity of daily life, sometimes for long periods of time. Even the simplest task can become a hurdle to overcome, and expending a small amount of energy can put a person right back in bed.

The cause of CFS is not currently known. Some research is devoted to trying to find the cause of CFS and is involved in a variety of testing including viral/immunological testing, breathing studies, neuropsychological testing, body temperature measurements and muscle fatigue evaluation[10]. Studies suggest that the nerves controlling heart rate function abnormally in patients with CFS. As we know, heart rate variability reflects the action of autonomic nervous system (parasympathetic and sympathetic). Therefore, we will measure the variability of heart rate in normal people and CFS patients to study the action of the autonomic

nerve system.

The investigation of heart rate variability was conducted to evaluate fractal dimension, entropy and nonlinearity of heart interbeat interval signals(IBI). The techniques we focused on were the correlation integral, phase space representation, fast Fourier transform, spectral synthesis method(SSM), and statistical hypothesis testing("bootstrapping").

CHAPTER 2

CHAOS AND FRACTALS IN HEART RATE VARIABILITY

2.1 Introduction

Chaos and fractals are associated with the discipline of nonlinear dynamics: the study of systems that respond disproportionately to stimuli. The theory of nonlinear dynamics provides insights into the phenomenon of epidemics, the kinetics of certain chemical reactions and the changes in the weather. Under some circumstances deterministic nonlinear systems--those that have only a few simple elements--behave erratically, a state called chaos. The deterministic chaos of nonlinear dynamics is not the same as chaos in the dictionary sense of complete disorganization or randomness. Nonlinear chaos refers to a constrained kind of randomness, which , remarkably, may be associated with fractal geometry. Fractal structures are often the remnants of chaotic nonlinear dynamics. Wherever a chaotic nonlinear process has shaped an environment (the seashore, the atmosphere, a geologic fault), fractals are likely to be left behind (coastlines, clouds, rock formations). At first the mathematics of fractals developed independently of nonlinear dynamics, and even today the connections between the disciplines are not fully established[1].

The term fractal, presented by the mathematician B. Mandelbrot[11], is currently used in three related contexts: geometric, temporal (dynamical), and statistical. In the most general terms, fractals are defined by a property called self-

similarity. Fractal objects are composed of subunits that resemble the larger scale shape. These subunits in turn are composed of yet smaller units that also look similar to the large ones, and so on. Fractals, therefore, do not have a single length scale, but rather have structure on multiple scales of length. The notion of self-similarity has also been extended into temporal and statistical domains. A temporal fractal is a process that does not have a characteristic scale of time, analogous to a geometric fractal that lacks a characteristic scale of length. Instead, fractal processes have self-similar fluctuations on multiple scales of time. This property is reflected by a type of broadband frequency spectrum, i.e., one having multiple frequencies. The concept of temporal fractals is closely related to that of "chaos". One example of fractal geometry is the irregular structure of the mammalian lung, where there is a self-similar distribution of scale sizes across multiple generations of branchings[12].

The concept of fractals, therefore, applies not only to complex physiological systems with self-similar structures and multiple scales of length, but also to certain dynamic processes which have fluctuations over multiple scale of time.

2.2 Fractal in Heart Rate Variability

A. The Heart's Fractal-like Anatomy

A number of cardiac structures have a self-similar or fractal-like appearance[13]. Examples of this nonlinear architecture include the coronary arterial and venous trees, the chordae tendineae, certain muscle bundles, and the His-Purkinje network(Figure2.1). The latter provides an efficient way of distributing

the depolarization stimulus to the ventricles. Recently, there has been interest in modeling the electrical genesis of the QRS complex using a fractal-like conduction system, as well as for studying alterations in the frequency content of the normal QRS due to changes in His-Purkinje geometry or in myocardial conduction. Abboud and colleagues[1][14] have shown that slow conduction in myocardial cells activated by such a fractal network can lead to "late potentials" or to selective attenuation of higher frequency content of the QRS, simulating changes seen in ischemic coronary syndromes.

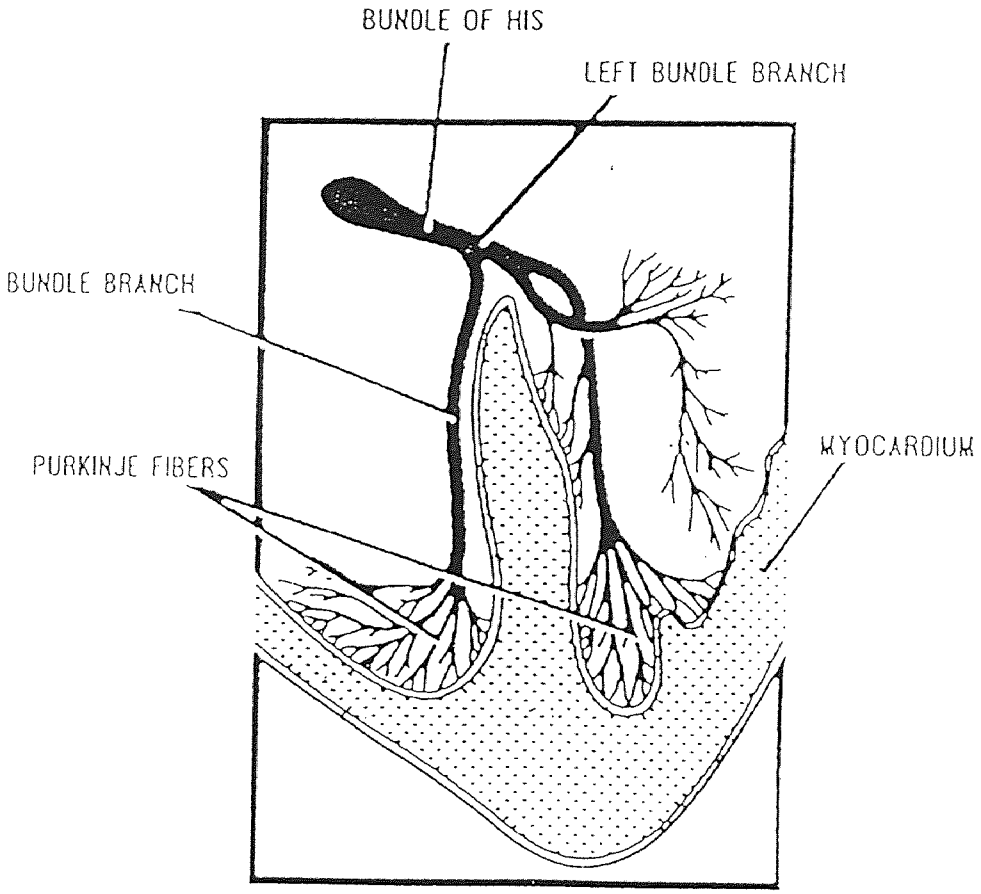

Figure 2.1 The self-similar branchings of the His-Purkinje system constitute a fractal-like network.

Idealized (computer-generated) fractals have infinite scales of length and literally have no smallest scale. Physiologic fractals are obviously bounded at both the upper and lower ends. However, the definition of a fractal does not require infinite scales of length. Furthermore, it is also apparent that physiological fractals are not identical on different scales of magnification. However, structures such has the tracheo-bronchial tree and the His-Purkinje system do maintain a similarity of dichotomous branching for which the term "fractal-like" is mathematically appropriate[1][11][13]. Interconnections between branches of the His-Purkinje system, which makes the system more than a simple branching structure, also do not undermine the fractal-like nature of the geometry.

B. The Heartbeat Interval is a Temporal Fractal

As noted, the fractal concept can be extended from geometry to dynamics. In this latter context, we will describe certain complex processes that do not have a characteristic scale of time. The regulation of the heart rate may be one such fractal processes[15]. The conventional opinion considered the normal heartbeat as highly regular ("regular sinus rhythm") because palpation of the pulse and observation of the electrocardiogram in a healthy individual gives the appearance of metronomic regularity. However, actual measurements of interbeat interval fluctuations reveal quite a different impression.

A pattern emerges from both the heart rate and heartbeat interval data plotted over several different time scales. See Figure2.2[15]. We find more rapid fluctuations whose range and sequence appear to be similar to the original, longer time-series plot. The beat to beat fluctuation on different time scales appear to be

just like the branches of a geometric fractal. Therefore, the heartbeat interval is a temporal fractal. This observation suggests that fractal mechanisms may be involved in the regulation of heart rate variability.

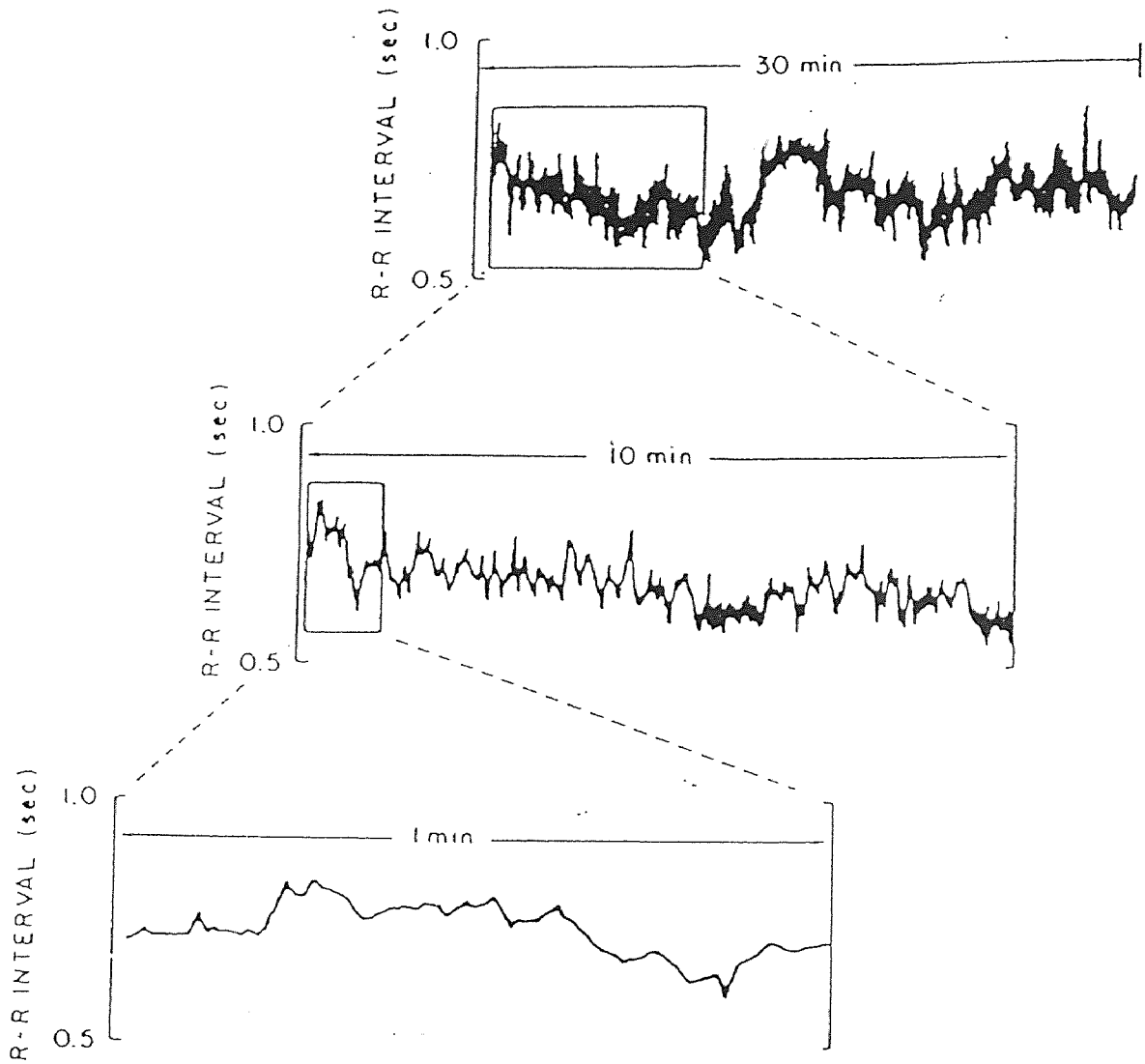

Figure 2.2 Normal sinus rhythm is not regular, but rather shows apparently erratic fluctuations across multiple time scales.

2.3 Fractal Dimension and Measurement

A. Fractal Dimension

Because a fractal is composed of similar structures of ever finer detail, its length is not well defined. If one attempts to measure the length of a fractal with a given ruler, some details will always be finer than the ruler can possibly measure. As the resolution of the measuring instrument increases, therefore, the length of a fractal grows.

Because length is not a meaningful concept for fractals, mathematicians calculate the "dimension" of a fractal to quantify how it fills space. The familiar concept of dimension applies to the objects of classical, or Euclidean,geometry. Lines have a dimension of one, circles have dimension of two and spheres have dimension of three. Fractals, however, have noninteger (fractional) dimensions. A fractal line--a coastline,for example-- has a dimension between one and two. Likewise a fractal surface --a mountain, for instance--has a dimension between two and three. An another well-known fractal object is the Cantor set whose dimension is 0.6039 (Figure 2.3)[16].

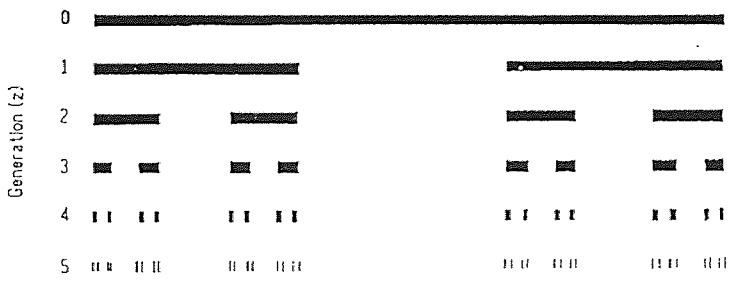

Figure 2.3 Construction of the Canton set by removing the middle third from each line segment between successive generations.

The initial stage (z=0) of the Cantor set is a line segment of unit length. The next stage (z=1) is obtained by discarding the middle third of the line, leaving the two intervals {0,1/3} and {2/3,1}. The z=2 stage is obtained by removing the middle third of each of the two intervals, leaving the four intervals {0,1/9}, {2/9,1/3},{2/3,7/9},{8/9,1} as shown. Repeating this process ($z\rightarrow\infty$) eventually produces the Cantor set[17]. At each stage, the number of intervals that are left behind increases, but they become small quite quickly. There are $2=2^1$ intervals of length 1/3 after the first removal, 2^2 intervals of length $1/3^2$ after the second, 2^3 of length $1/3^3$ after the third, and so forth. Thus, the number of intervals at each stage of the construction is 2^n and length of intervals is $1/3^n$.

To see how we can get the fractal dimension from a fractal structure, let us investigate the notion of dimension of lines, squares, and cubes more thoroughly. One way to realize that these objects have different dimensions is to do the following. A line is a very self-similar object: It may be decomposed into $n=n^1$ little "bite-size" pieces, each of which is exactly 1/n the size of the original line and each of which, when magnified by a factor of n, looks exactly like the whole line. On the other hand, if we decompose a square into pieces that are 1/n the size of the original square, then we find we need n^2 such pieces to reassemble the square. Similarly, a cube may be decomposed into n^3 pieces, each 1/n the size of the original. See Figure 2.4. Therefore, the dimension may be easily determined as follows: The exponent in each of these cases is precisely the dimension.

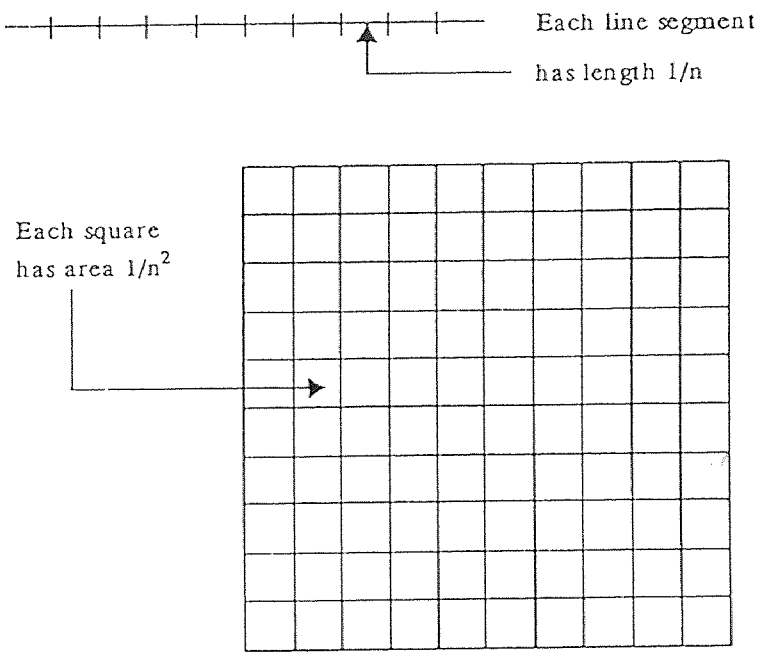

Figure 2.4 Calculating the dimentions of a line and a square

In these simple cases, it is trivial to read the exponent and find the dimension. For fractals, this is not always as easy, so let us formalize this procedure. One way to find the exponent in these three cases is to use the logarithm of the number of constituent pieces into which the object has been subdivided. For a line, we find

$$\log (\text{number of pieces}) = \log (n^1) = 1 \log n$$

For a square,

$$\log (\text{number of pieces}) = \log (n^2) = 2 \log n$$

and for a cube,

$$\log (\text{number of pieces}) = \log (n^3) = 3 \log n$$

We noticed the log (number of pieces) is equal to the dimension multiplied by log n.The n is called the magnification factor. If we divided the logarithm of the number of pieces by the logarithm of this magnification factor, we obtain the

dimension. That is, the dimension D is given by the formula

$$D = \frac{\log(\text{number of pieces})}{\log(\text{magnification})}$$

For a line, we find

$$D = \frac{\log n^1}{\log n} = 1$$

For a square,

$$D = \frac{\log n^2}{\log n} = 2$$

and for a cube,

$$D = \frac{\log n^3}{\log n} = 3$$

Each of these calculations was easy because the magnification factor in each case was n. But what about the Cantor set? Recall that at the any stage of the Cantor set the interval could be magnified by a factor of 3^n to produce the whole line. Therefore the magnification factor is 3^n, and the number of intervals at each stage is 2^n. Therefore, the dimension of the Cantor set is

$$D = \frac{\log 2^n}{\log 3^n} = 0.6039$$

B. Dimension of Fractal Time Series

The fractal dimension determined from a process in time yields information on temporal correlations in the data. Thus, the observation of such a fractal dimension can sometimes help in revealing the mechanism that produced or maintains the observed pattern in a system.

The fractal dimension is also called the attractor dimension. The attractor is used to describe the object on which the trajectories of a chaotic system accumulate. An attractor could be defined to be n-dimensional where n is not an integer. The fractal dimension can be computed from several different measures. The capacity, information dimension, and correlation dimension are used widely.

The capacity is the simplest type of dimension. It is computed as follows. Cover an attractor with volume elements each with radius r. Let N(r) be the number of elements needed to cover the attractor. As r becomes smaller, the sum of the elements approaches the attractor. The capacity D_{ca} is obtained by solving the following equation:

$$D_{ca}=\lim_{r\to 0}\frac{\log(N(r))}{\log(1/r)}$$

The information dimension is a probabilistic type of dimension. The computation is the same as for capacity: a covering of N(r) volume elements each with radius r. The information dimension Di is defined by

$$D_i=\lim_{r\to 0}\frac{\log s(r)}{\log(1/r)}$$

where

$$S(r) = -\sum_{i=1}^{N(r)} P_i \log P_i$$

The correlation dimension D_c is another probabilisic type of dimension. The measure is obtained by considering correlation between points of a time series on an attractor. D_c is defined by:

$$D_c = \lim_{r \to 0} \frac{\log c(r)}{\log r}$$

where $c(r) = \lim 1/N^2$ {the number of pairs of points x_i, x_j such that $|x_i - x_j| < r$}.

CHAPTER 3

CALCULATION OF DIMENSION AND ENTROPY

3.1. Introduction

Chaotic dynamic systems have an attractor in phase space which is termed strange[18]. An attractor is a subset of the dynamical system, that "attracts" phase points from other regions of the phase space in the basin of the attractor. This attractor may have a dimension different from the space in which the attractor is embedded. There are several measures that can be used to describe the strangeness of attractors. Dimension and entropy are two of the most useful methods.

The dimension of the attractor is an important feature in chaos. The development of algorithms for estimating the dimension of an attractor directly from a time series has been an active field of research over the last decade. The objective of these algorithms is to estimate the fractal dimension of a hypothesized strange attractor in a reconstructed state space. The correlation dimension developed by Grassberger and Procaccia[19] considers the statistics of distance between pairs of points. The correlation dimension measures extent of correlation between the data points.

The entropy measures the amount of information needed to specify the state of a system. If we say the dimension indicates how many past values of the system are needed to predict the future, then we can say the entropy indicates how well the future can be predicted given the past. The algorithms to calculate the entropy

are closely related to those of dimension. In general, entropy is calculated by embedding a time series, finding a set of instances where the recent history of the time series is similar, and quantifying the probability distribution of the near future of the time series after the set of instances.Both techniques have a common starting point: embedding the time series.

3.2 Embedding

For characterizing and understanding the dynamics on a finite-dimensional attractor the first step in analyzing such experimental data is a reconstruction of the observed dynamics.

The past behavior of the time series contains information about the present state. This information can be represented as a delay vector of dimension m. In other words, a scaler time series x_i can be embedded in an m-dimensional space by constructing the vector time series:

$$x_i \quad \text{vs.} \quad (x_i, x_{i-1}, \ldots. x_{i-(m-1)})$$

That is, each data point, along with m-1 previous points, becomes one dot in a m-dimensional space. This is called embedding the data. The goal of the embedding is to use the immediate past behavior of the time series to reconstruct the current state of the system.

m is called the embedding dimension and describes the space in which the object is contained. When m is large enough, it can be shown that this embedding preserves the topological properties of the original system that generated the measured time series x_i. Therefore, the embedding dimension must be correctly

chosen so that the original system and its reconstruction are qualitatively equivalent. There is no hard and fast rule for picking m. Takens proved that the embedding dimension m should be at least 2D+1 for a system that is found to have dimension D[20].

3.3 Correlation Dimension

For a dynamical system with a m-dimensional phase space, let $\{x_i\}_{i=1}^{N}$ be the points of a time series on the attractor. Cover the attractor with volume elements (spheres,cubes,etc.) each with radius r. The correlation dimension is defined by :

$$D_c = \lim_{r \to 0} \frac{\log c(r)}{\log r} \tag{3-1}$$

where c(r), correlation integral is obtained by considering correlations between points of a time series on the attractor and is given by:

$$c(r) = \lim_{r \to 0} \frac{1}{N^2} \sum_{i,j=1}^{N} H(r - |x_i - x_j|) \tag{3-2}$$

Here, N is the total number of data points, x_i, x_j are embedded points, and H is the Heaviside function : H(x)=0 if x<0, H(x)=1 if x>0. The correlation integral c(r) is the proportion of pairs of data points in the embedding space whose distance $|x_i - x_j|$ is less than r. Therefore, we can also describe c(r) as follows:

$c(r) = \lim 1/N^2$ { the number of pairs of points x_i, x_j such that $|x_i - x_j| < r$} (3-3)

c(r) measures the extent to which the presence of one data point affects the position of the other data points.

The formula in (3-1) will now be derived as follows: An attractor is covered by volume elements with radius r. Let M(r) be the number of volume elements needed to cover the attractor. As r is made smaller, the sum of the volume elements approaches the volume of the attractor. Then for small r, the number of volume elements needed to cover the attractor is inversely proportional to r^D[19], that is

$$M(r) \sim r^{-D} \tag{3-4}$$

where D is the dimension of the attractor. Let n_i be the number of data points which lie within the ith element. Since c(r) counts the number of pairs of data points which lie in the volume elements, the n_i points form n_i^2 pairs of points. Therefore, the total number of pairs of points in the M(r) volume elements is

$$\sum_{i=1}^{M(r)} n_i^2$$

Substituting into (3-3), it follows that

$$c(r) \sim \frac{1}{N^2} \sum_{i=1}^{M(r)} n_i^2 = \frac{M(r)}{N^2} \frac{\sum_{i=1}^{M(r)} n_i^2}{M(r)} = \frac{M(r)}{N^2} \langle n^2 \rangle \tag{3-5}$$

where angular brackets denote an average of n_i^2 over all occupied elements.

For small n_i, or small r

$$\frac{M(r)}{N^2}\langle n^2\rangle \sim \frac{M(r)}{N^2}\langle n\rangle^2 = \frac{M(r)}{N^2}\left[\frac{\sum_{i=1}^{M(r)} n_i}{M(r)}\right]^2$$

$$= \frac{1}{N^2 M(r)}\left[\sum_{i=1}^{M(r)} n_i\right]^2 = \frac{1}{N^2 M(r)} N^2 = \frac{1}{M(r)} \qquad (3\text{-}6)$$

where $\sum n_i = N$ has been used. From (3-5) and (3-6) we have

$$c(r) \sim \frac{1}{M(r)} \qquad (3\text{-}7)$$

Using (3-7) and (3-4), a important relationship can be derived:

$$c(r) \sim r^D \qquad (3\text{-}8)$$

c(r) behaves as a power of r. If the attractor is a line, c(r) should be directly proportional to r. If it is a surface, c(r) should be proportional to r^2. In general c(r) should be proportional to r raised to the D power for an attractor of dimension D.

From (3-8), (3-1) follows. Formula (3-1) shows that correlation dimension D_c is the slope of the log c(r) versus log r relation. We calculate the slope using a least square fit

$$slope = \frac{\sum_{i=1}^{N} x_i y_i - \sum_{i=1}^{N} Y_i \sum_{i=1}^{N} x_i}{\sum_{i=1}^{N} x_i^2 - \left(\sum_{i=1}^{N} x_i\right)^2} \qquad (3\text{-}9)$$

where the x_i correspond to log r and y_i correspond to log c(r).

A log-log plot which is made from a heartbeat interval signal is shown in

Figure 3.1. It is clear from the figure that there is a limited range (between r_a and r_b) where the slope is approximately constant and only data from this range should be used to estimate D_c. Unfortunately, there is currently no best technique available to detect the useful range of r automatically. Kaplan suggested selecting r_a and r_b so that $c(r_a)$= 0.5% of maximum c (r) and $c(r_b)$ = 75% of maximum c(r)[21]. Taken suggested only an upper cutoff value[22], and $c(r_a)$= 0. We selected the latter suggestion and set the upper cutoff to 75%.

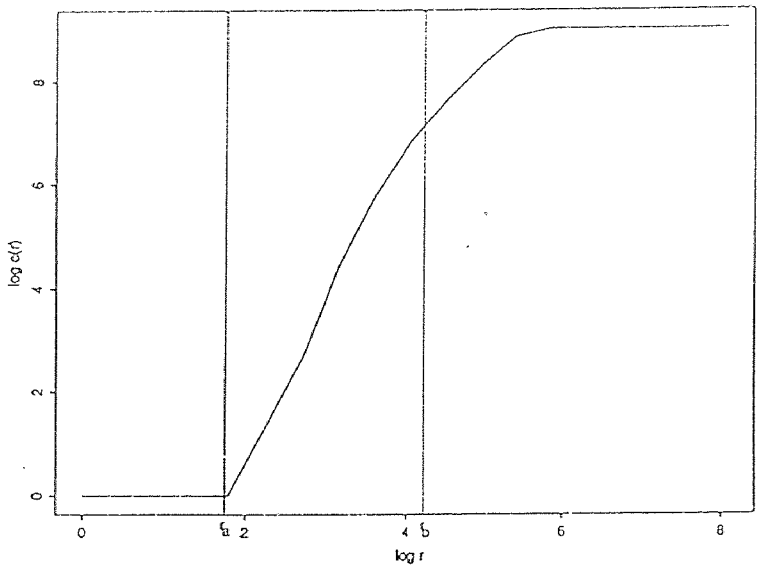

Figure 3.1 Correlation intergral C(r): log-log plot for one value of m

For a deterministic system, D_c reaches a limiting value as embedding dimension m is increased. This limiting value can be taken as the dimension of the system's attractor. For a random system D_c will increase as m is increased. However, even for a deterministic system, D_c will increase with m if m is small (See Figure3.2). When m=1,2,3,4, the slope of the curve obviously increased with increasing m. When m is larger than 5, the curves are relatively parallel.

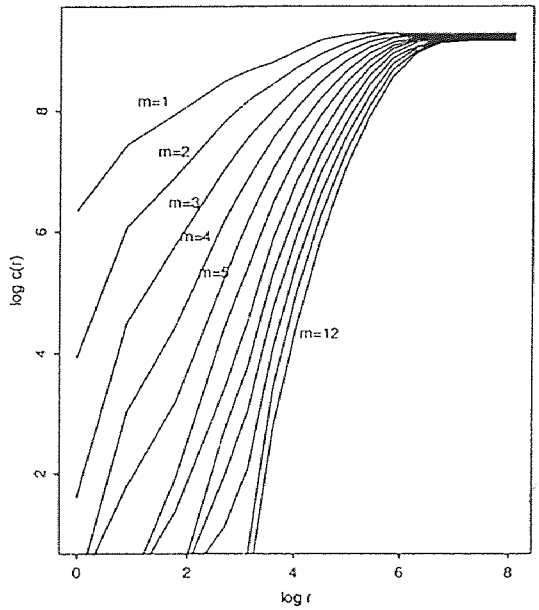

Figure 3.2 Correlation integral C(r): log-log plot . The values of m are m=1(top curve), 2,3 4,..... 12(buttom curve)

How large should the embedding dimension m be? This was discussed in section 3.2 where we set $m \geq 2D_c+1$. But we don't know the D_c before the embedding has been performed. In practice, m is often selected by repeating the calculation for many values of m, and selecting an m in the range where the slope of the correlation integral curve does not vary strongly with m (range of parallel curves).

In our study, we measured the correlation integral for the embedding dimension from m=1 to m=12 to get a group of curves. Then we selected m=8 according to the two rules: $m \geq 2D_c$ and the slope of the curve independent of m.

3.4 Phase Space Plot and Entropy

A.Phase Space Plot

One of the essential differences between dynamic chaotic and predictable

behavior is that chaotic trajectories continually generate new information, whereas predictable trajectories do not. Therefore, another way to quantify complexity of a dynamic chaotic system is by investigating the predictability of the system, which deals with the amount of information needed to predict the future state of system given its past. This can be performed by embedding the time series with embedding dimension m=2, or making a phase space delay plot. Each data point x_i was plotted on the Y-axis against the previous value x_{i-1} on the x-axis to produce a phase space delay plot (See Figure 3.3).

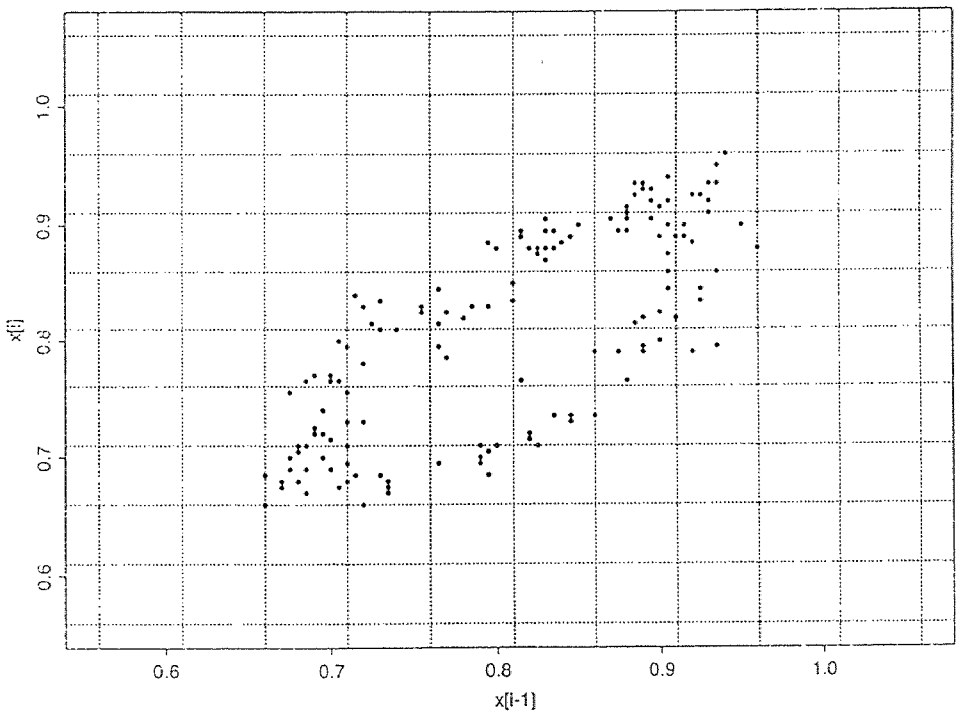

Figure 3.3 A phase space delay plot for a IBI data

The plot illustrates the two aspects of the system: 1) the point-to-point

dispersion (changes in x_i at a given value of x_{i-1}), which is reflected in the scatter of values on the Y-axis for a certain value of x. It measures instantaneous changes in the point-to-point relationship of the time series; 2) the overall range of the data set, which is reflected in the absolute extent of dispersion of points on both the X and Y-axes. It measures the overall variation of the time series.

In order to quantify these two aspects we can look at the distribution of all embedding data in the overall range (along the X-axis) and the distribution of partial embedding of the data on the y-axis at a particular x value. If this distribution is narrow (i.e., the embedding data are similar), then the system is predictable. If the distribution is wide, the system is less predictable. Entropy is used to quantify the width of the distribution.

B. Entropy

The calculation for entropy is started by dividing the phase space plot into m×m boxes (see Fig. 3.3). The size of the box is determined by intervals of the X-axis and the Y-axis. The boxes are labelled box_{ij}. The i corresponds to the ith interval of the X-axis and the j corresponds to the jth interval of the Y-axis. Let the number of points in box_{ij} be x_{ij}. Two entropies must be calculated: overall entropy and partial entropy at a given interval of the X-axis. The overall entropy quantifies the dispersion of all points in the overall range. The partial entropy quantifies the dispersion of partial points at certain range of the X-axis.

For overall entropy, we consider a sequence $x_i(m)$ of m successive measurements made at the ith interval of the X-axis, $x_i(m)=x_{i1},x_{i2},.....x_{im}$. Let $P(x_i(m))$ be the probability of the sequence $x_i(m)$, that is

$$P(x_i(m)) = \frac{x_i(m)}{\sum_{i=1}^{m}\sum_{j=1}^{m} x_{ij}}$$

We also know

$$\sum_{i=1}^{m} P(x_i(m) = 1$$

We can plot the distribution of probability $P(x_i(m))$ in each interval of the X-axis (See Figure 3.4).

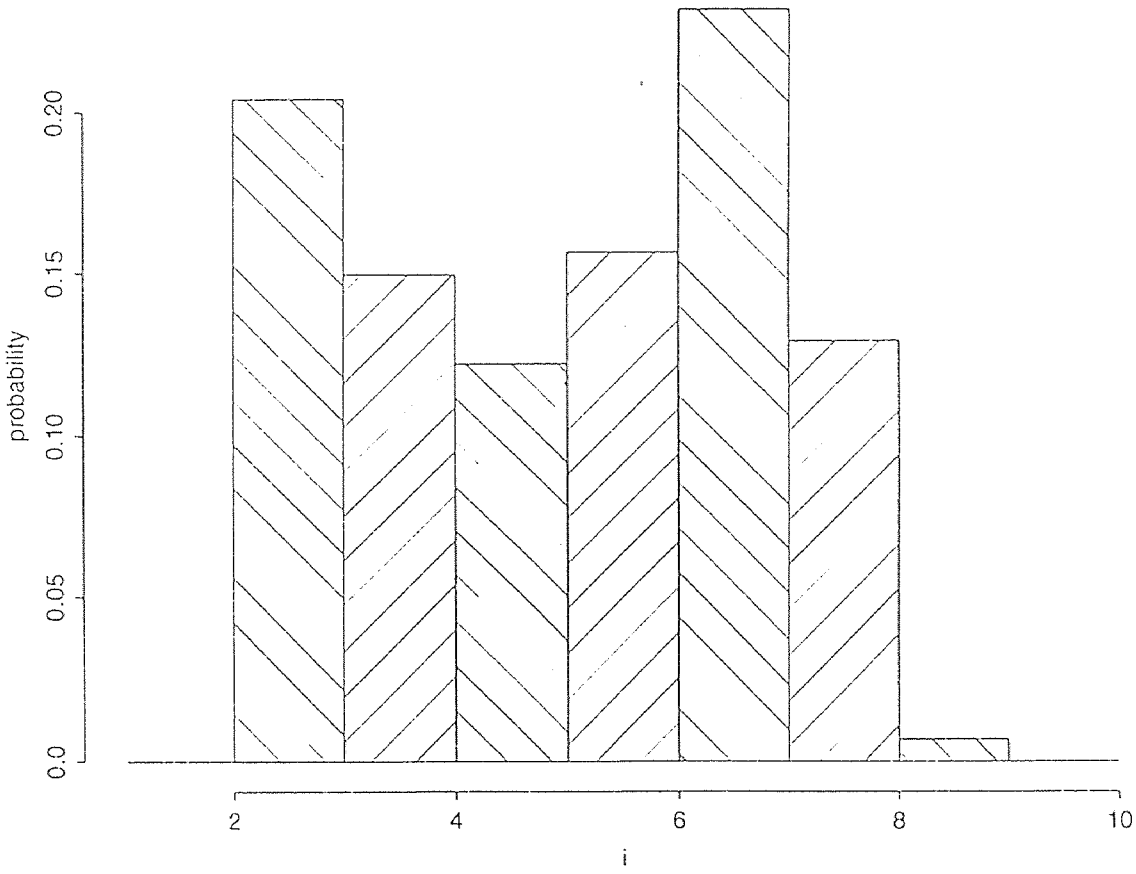

Figure 3.4 The distribution of probability $p(x_i(m))$ in each interval of the x-value.

The overall entropy E_o is then given by the following:

$$E_o = -\sum_{i=1}^{m} P(x_i(m) \log P(x_i(m)) \tag{3-10}$$

For partial entropy,we still need to determine $x_i(m)$ at a given i value, let $P(x_{ij})$be the probability of points x_{ij}, that is

$$P(x_{ij}) = \frac{x_{ij}}{x_i(m)} \tag{3-11}$$

It is clear that

$$\sum_{j=1}^{m} P(x_{ij}) = 1$$

We can also plot the distribution of probability $P(x_{ij})$ in each interval of the Y-axis at a given i (see Fig.3.5).

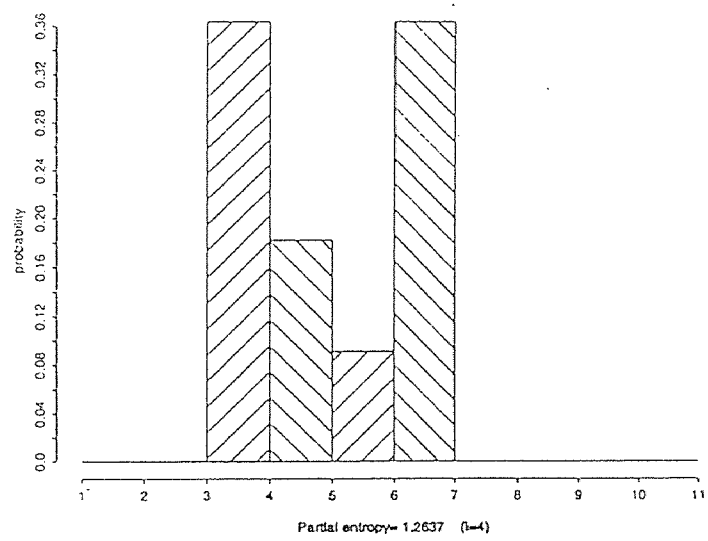

Figure 3.5 The distribution of probability $P(x_{ij})$ in each interval of the Y-axis at i=4

The partial entropy is then given by the following:

$$E_p = -\sum_{j=1}^{m} P(x_{ij}) \log P(x_{ij}) \qquad (3\text{-}12)$$

It is obvious that probabilities $P(x_i(m))$ and $P(x_{ij})$ depend on the width of the box. Different entropies are obtained from different box sizes. Therefore, we must keep the same box size for every data set in order to make the results comparable.

3.5 Nonlinear Structure Detection

We will now consider whether a given time series contains nonlinear structure that might be exploited by a nonlinear prediction algorithm. Classical statisticians have long considered tests for nonlinearity, and are becoming increasingly aware of low-dimensional chaos. Theilers has described an approach for testing nonlinear structure in time series, namely,the method of surrogate data[9].

The method of surrogate data is a statistical hypothesis testing which includes three steps: first start with a null hypothesis that the time series is linearly correlated noise, then given a raw time series, generate an ensemble of surrogate data sets which share given properties of the original data (such as mean, variance, or Fourier spectrum) but are otherwise random, and finally compute the discriminating statistic (dimension, Lyapunov,etc.) for the original and for each of the surrogate data sets. If the difference of the value between the original time series and surrogate data sets is significant, then the null hypothesis is rejected and

nonlinear structure in the original data set is detected. The techniques which are involved in this method are generating surrogate data and computing significance.

A. Generating surrogate data

There are several way to generate the surrogate data . We use an algorithm which involves randomizing the phase of a Fourier transform[9]. This method is numerically stable. This algorithm is based on the null hypothesis that the data come from a linear gaussian process. The surrogate data are constructed to have the same Fourier magnitude spectrum as the raw data. A practical way to do this is to take a Fourier transform of the raw data, and randomize the phases (while keeping the magnitudes intact). The Fourier transform has a complex amplitude multiplied by $e^{i\varnothing}$, where $\varnothing$ is independently chosen for each frequency from the interval [0, 2π]. In order for the inverse Fourier transform to be real (no imaginary components), we must have symmetrical phases, so that $\varnothing$ (f) = -$\varnothing$(-f). Finally we take the inverse Fourier transform. The resulting time series is the surrogate data which will have the same power spectrum as the raw time series, but will in other respects be random.

B. Computing significance

We compute the correlation dimension for the original time series and each surrogate data set. Let the value of D for the original time series be D_o and the value of D for the ith surrogate data be D_i. Let D_s and σ_s be the mean and standard deviation of the set $\{D_i\}$. We define our measure of "significance" by the difference between D_o and D_s divided by σ_s[9]:

$$S=\frac{|D_o-D_s|}{\sigma_s} \tag{3-13}$$

If $|D_o - D_s| >> \sigma_s$, then we can be confident that there is significant nonlinear structure in the time series that is not captured in the linear stochastic surrogate data sets. This calculation is similar to a two tailed t-test. We can look up the p value from the t-value table in terms of the S value. If $p<0.05$ there exists a significant difference between the raw data and surrogate data. Otherwise there is no significant difference between these two data sets.

CHAPTER 4

METHODS AND RESULTS

4.1 Methods

Chronic Fatigue Syndromes (CFS) is a chronic disabling illness characterized by fatigue which is not the result of any medical conditions known to cause fatigue. The cause of CFS is not currently known. Because CFS patients frequently have symptoms including palpitation, diarrhea and urinary frequency/nocturia, an evaluation of autonomic nervous function might be necessary. Some earlier research on heart rate responses to exercise suggested autonomic dysfunctions in CFS. The present study on heart rate variability response to paced breathing addresses this question.

Because heart rate varies with respiration, many techniques exist to quantifying the relationship between heart rate variability and respiration. Some studies have shown that all the variability in heart rate that occurs at the respiratory frequency is due to vagal activity[2][23]. Sisto[24] demonstrated the difficulty of deriving a relationship between natural respiratory and heart rate because natural respiration is not regular and stable. Therefore, we used a paced breathing protocol which improved the situation. Paced breathing is a method where subjects are forced to breathe at a certain rate. We performed the test using two groups: normal controls and CFS patients. The experimental procedure included selection of subjects, data collection, and data analysis.

4.1.1 Subjects

12 healthy subjects and 12 CFS patients took part in this study. These two groups were age and gender matched. Subjects were excluded from the study if they were on sympatholytic or sympathomimetic medications, and subjects were restricted from having caffeine or chocolate one hour before test. Two of the control subjects reported hayfever, one had mitral valve prolapse, one was pregnant and one was taking fluoxetine. Seven of the CFS group were taking medication.

4.1.2 Experimental Procedure

The subjects were asked to breathe in a normal unpaced breathing mode and at three controlled rates of 8,12,and 18 breaths per minute performed in both sitting and standing postures. Each posture lasted 8 minutes. During each 8 minutes test, the subjects breathed naturally in the first 2 minuets in order to become stable, followed by breathing at 8, 12, and 18 breaths/min. Each stage lasted 2 minutes. Breathing rate was controlled by a view box containing a column of lights that rose and fell at the desired breathing rate. The participant was instructed to match his/her breathing rates with the rate with which the light proceeded up and down the column. A light moving up directs subjects to breath in and a light moving down directs subjects to breathe out.

Full ECG and respiratory signals from each participant were monitored during the paced breathing protocol.

4.2 Data Processing

4.2.1 Data Collection

The ECG and respiratory signals were recorded by a 2-channel pneumograph (RESP1, UFI Morro Bay, CA). Data was collected for 2 minutes per rate starting in the sitting position. A personal computer with internal A/D converter supported by Dash-16 streamer software was used to digitize signals at a sampling frequency of 200 Hz and store the 2-channel signals sequentially. Then, data were transferred from the PC to a Sun Sparc workstation for processing and analysis.

4.2.2 Data Processing

All the data processing was performed on a Sun workstation using the Splus language. The heart rate variability signal was formed by detrending the signals, detecting R-waves, and correcting abnormal data points. The very low frequency components contained in a signal are sometimes an artifact caused either by the instruments used to acquire the signal or by such effects as the movement of subjects which shift the signal up and down. We eliminated those very low frequencies by using a locally weighted robust regression procedure[25]. Then, R-waves were detected from ECG signals (Figure 4.1(a)) by a software algorithm. Taking the difference in time between successive R-waves (Figure 4.1(b)) we obtained the R-R interval signal which is also called interbeat interval (IBI) signal. (See Figure 4.1(c)).

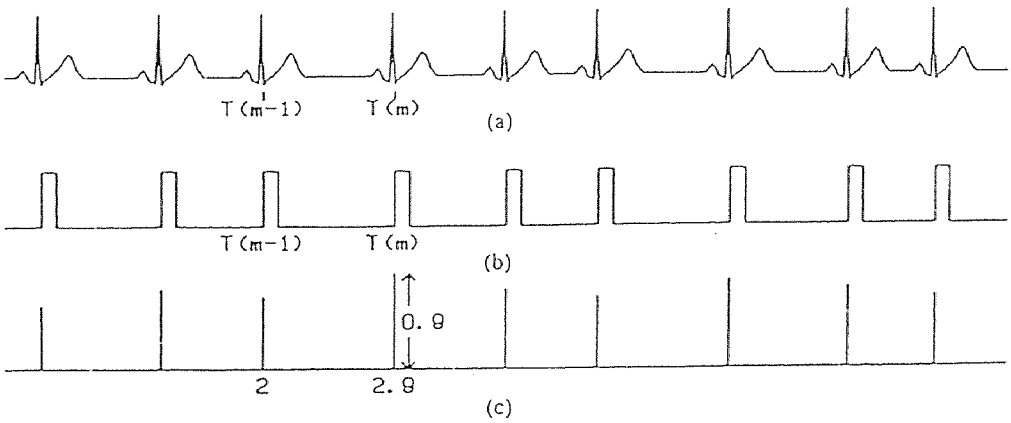

Figure 4.1 (a) ECG signal. (b) R-waves. (c) IBI values.

The IBI signals were viewed graphically to find the abnormal data points which will affect the analysis. There were a small number of abnormal R-R intervals caused mainly by body movements during the test. These abnormal intervals were corrected by either omitting or inserting beats. The number of data points corrected manually in this way was much less than the total number of data points so that the final result is not greatly affected. Some data sets have so many abnormal points so to cause the distortion of the signals. These data were discarded. We selected nine reliable data sets of each group to be used in our study. Each data set included six stages of data, that is, breathing at 8, 12, and 18 cycle/min in both sitting and standing postures. The resulting data sets (IBI signals) were analyzed by using the algorithms described in chapter 3.

4.3 Results

4.3.1 Correlation Dimension

A. Individual results

Figure 4.2 shows the data from one healthy control and one CFS patient. Both

signals were obtained during breathing at 8 cycle/min in the standing posture. The top panel shows interbeat interval (IBI) signals. TheY-axis reflects the length of the R-R interval and the X-axis represents the heart beat number. The middle panel shows the correlation integral c(r) vs. r (log-log plot) by using formula (3-2) with embedding dimension m=8. The bottom panel shows the calculation of correlation dimension D_c. The straight line in the figures is obtained by using a least-square fit (3-9). The slope of the line is the correlation dimension D_c. The value for the normal subject is 2.296 while the value for the CFS subject is 3.24. The data for all subjects are shown in Table (4.1).

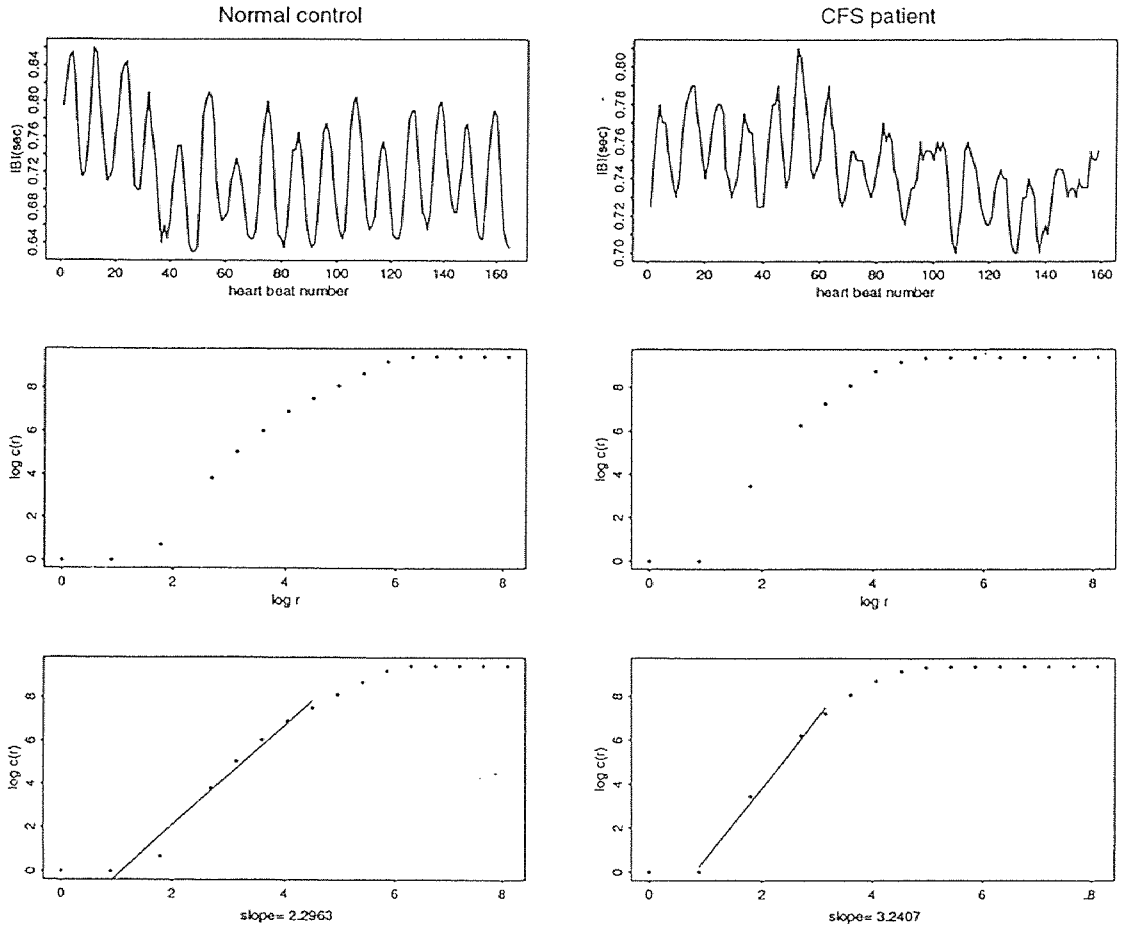

Figure 4.2 Correlation integral and correlation dimension for an IBI signals.

Table 4.1 Individual correlation dimension (* normal subject and #CFS patient)

Subject	Stage1	Stage2	Stage3	Stage4	Stage5	Stage6
1*	2.6883	2.4478	2.3754	2.4356	2.6517	3.1279
2*	2.4911	2.9100	3.1252	2.2963	2.4953	3.1174
3*	2.1407	3.2387	3.3031	2.5981	3.2954	3.5455
4*	2.4071	2.5543	3.3158	2.6702	2.4385	3.3939
5*	2.5107	3.4254	3.2453	2.4068	3.0676	3.3544
6*	2.0237	2.6619	2.7897	2.1918	2.5104	3.3414
7*	3.0641	2.3267	2.7298	2.2564	3.3708	3.3405
8*	1.9368	2.7211	3.0649	2.1656	2.9053	3.1035
9*	3.1092	2.8993	3.0594	2.3164	2.6461	2.8554
10#	2.6216	3.5502	3.4123	2.8121	3.1432	2.7931
11#	2.4283	3.3483	3.3522	2.4725	2.9411	3.5704
12#	2.7112	2.8247	2.9489	2.8268	2.3209	3.2876
13#	1.8866	2.1778	2.8551	2.2381	2.5112	2.5109
14#	2.1787	2.1740	1.7895	2.1695	2.4273	3.2621
15#	2.8066	2.7975	3.4296	3.2407	3.3611	4.0202
16#	2.9063	3.3637	3.2509	2.4436	2.6137	3.2729
17#	2.4995	3.1053	3.3019	2.9021	2.9789	3.5593
18#	2.4836	2.6750	4.2774	2.6033	3.0946	3.2493

B. Correlation dimension in different stages

Figure 4.3 shows the results from the six different stages for a normal subject. The left panel shows the results for breathing at 8,12, and 18 cycle/min while sitting. The right side is while standing. As the breathing rate increased from 8 to12 to 18 cycle/min, the straight line became more steep in both postures. The correlation dimension D_c is increased from 2.0237 to 2.7897 in sitting and from 2.1918 to 3.3414 in standing. This result for all subjects is shown in Table (4.1).

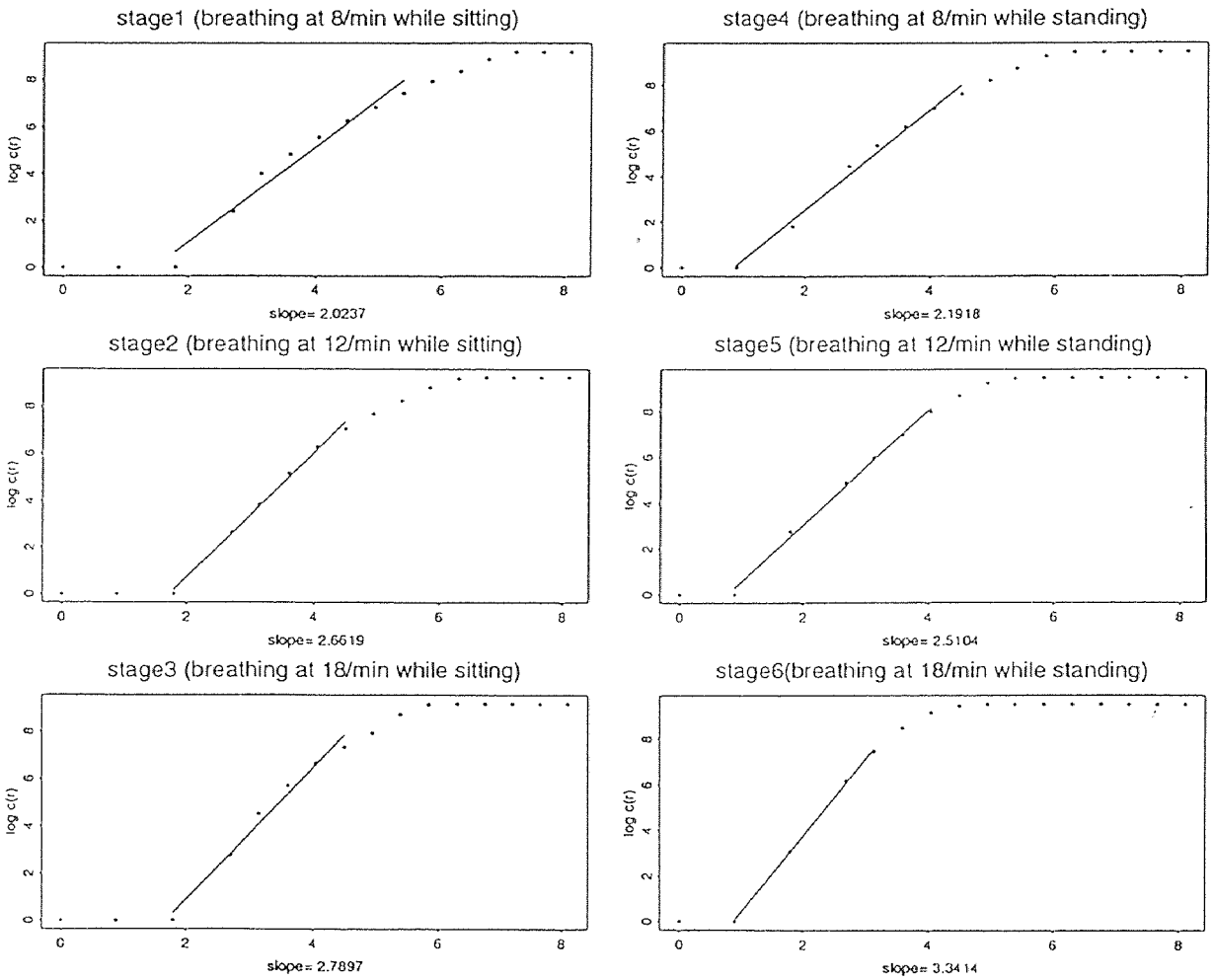

Figure 4.3 Correlation dimension for six stages for a normal subject.

C. Correlation dimension in different groups

Figure 4.4 shows the mean value of correlation dimension from normal and CFS groups for all 6 stages. The solid line describes the normal group and the dotted line demonstrates the CFS group. Each value for the CFS group is larger than the corresponding value for the normal group. Therefore, in every stage the CFS group has a larger correlation dimension than the normal group. Bars reflect the standard deviation of the data. The result of a t-test shown in Figure 4.4 shows that there was significant difference between these two mean values except for the sixth stage. Also,the curve is rising as breathing rate increases within each posture. This is also observed in each individual subject (See Table 4.1).

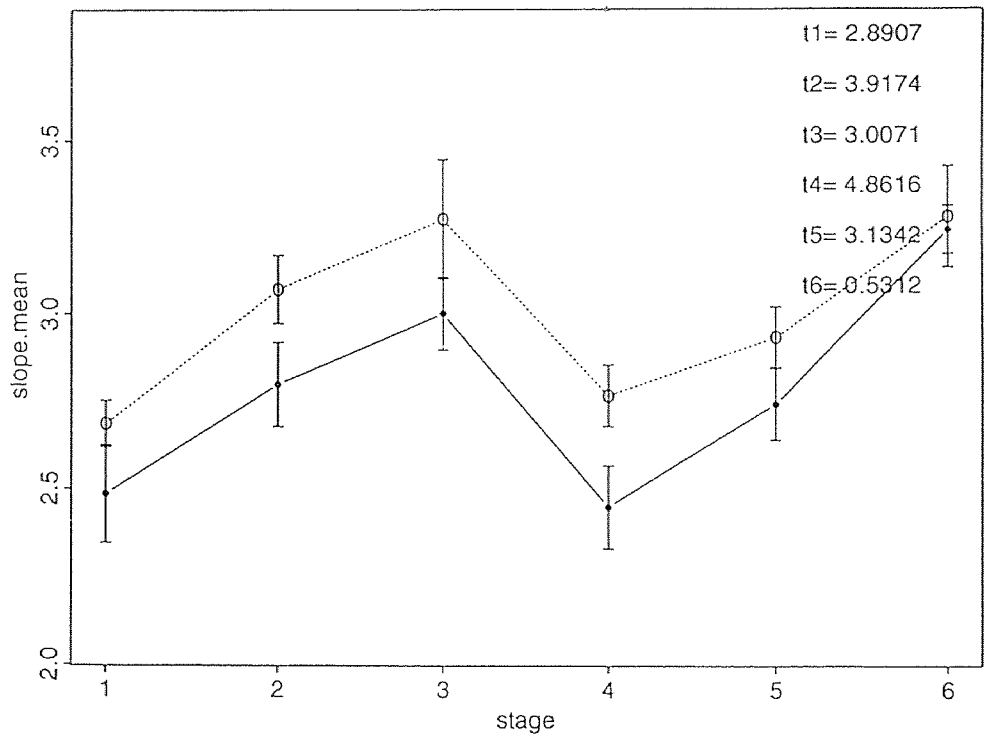

Figure 4.4 Mean of slope in normal and CFS subjects (——— normal,-------- CFS) stage1,2,3 are breathing at 8,12, and 18 cycle/min while sitting, stage4,5,6 are breathing at 8,12, and 18 cycle/min while standing.

4.3.2 Phase Space Plots and Entropy

A. Phase space plots

Phase space plots calculated from stage1 (breathing at 8/min while sitting) for 9 control subjects and 9 CFS patients are shown in Figure 4.5. Each heartbeat interval RR_i was plotted on the Y-axis against the previous value RR_{i-1} on the X-axis, where RR is the time from one R-wave of the ECG to the next and i is the interval number.

The dominant characteristic of the scatter of points in the CFS patients is that they are relative short and narrow. There is an obvious trajectory in the phase space plot of normal subjects while there is a less defined one for the CFS subjects. If we enlarge the picture we might see a small trajectory in the picture. Two points emerge from this observation: 1) the absolute extent of dispersion of points on the X-axis for controls is larger than that of CFS patients, which indicates that the overall heart rate variability is larger in normal people than in CFS subjects; 2) the extent of dispersion along the Y-axis at a given X-value for controls is more wide than that for CFS patients, which indicates the beat-to-beat variability is larger in normal subject than in CFS patients.

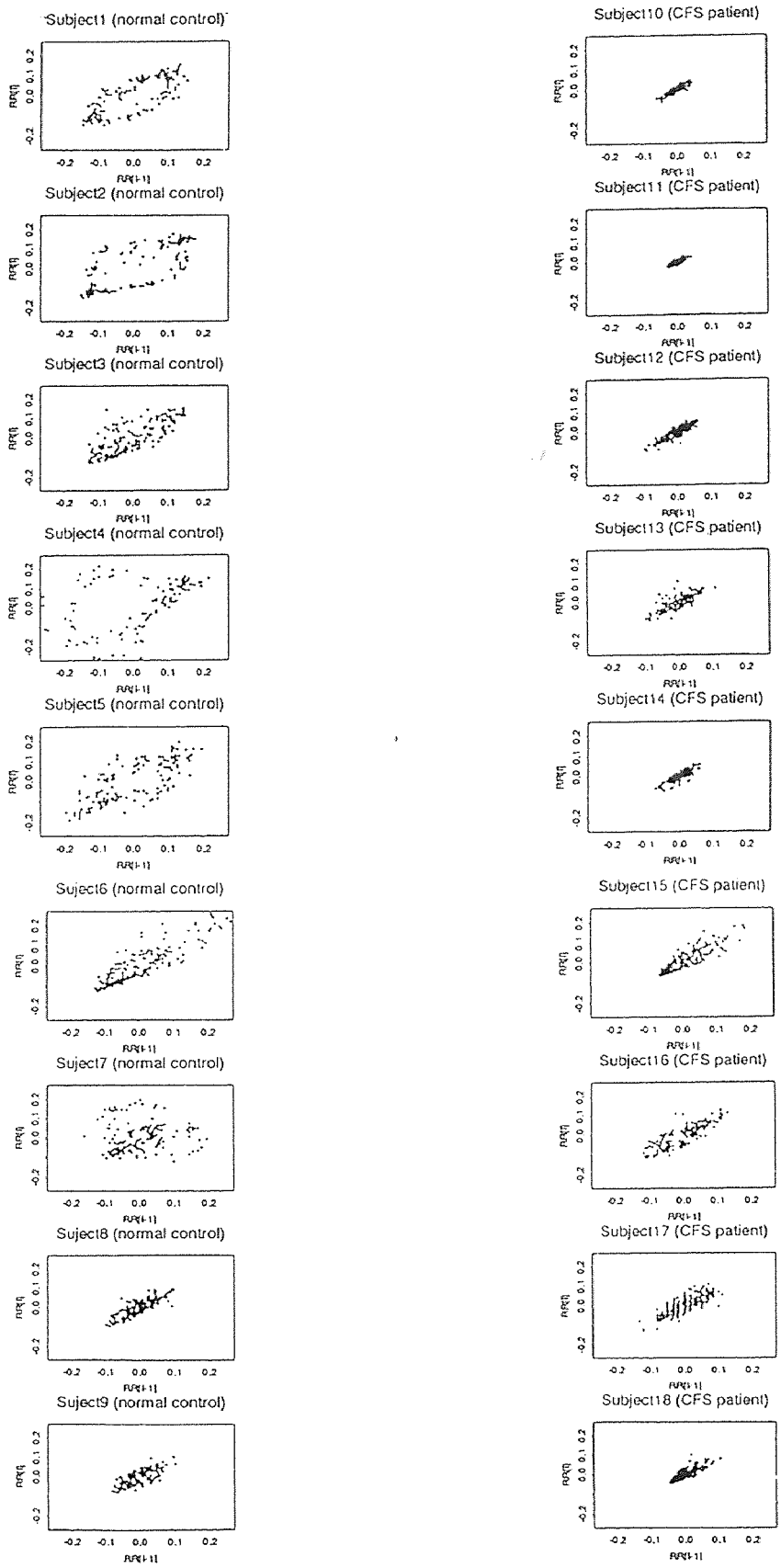

Figure 4.5 Phase space plots for nine normal subjects and nine CFS subjects.

B. Overall entropy

The overall entropy is used to quantify the dispersion of the overall range of data points. We divide the phase space plot into 20 intervals as shown in Figure 4.6 and count points in each interval.

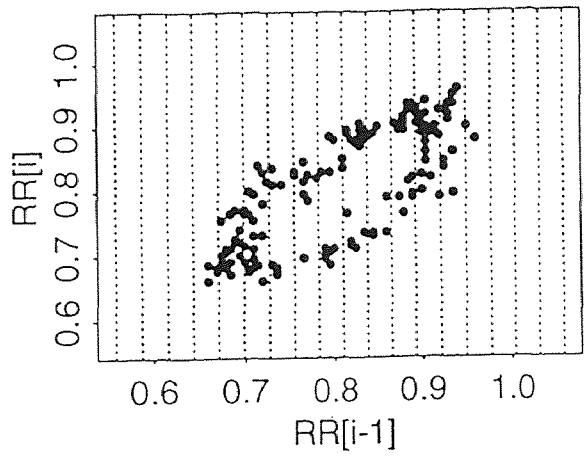

Figure 4.6 Phase space plot divided into 20 intervals along X-axis.

Let the number of points within the ith interval be x_i and the total number of point be x. The probability of x_i is

$$P_i(x_i) = \frac{x_i}{x}$$

We calculate the P_i for each interval and plot the distribution of P_i as shown in Figure 4.7.

Figure 4.7 shows the histograms of the probability distribution for the overall range of the data set from Figure 4.5 for subject1 and subject10. This figure demonstrates a big difference in the width of the distribution for the two subjects. The range of the distribution of the normal subject is almost twice that of the CFS subject.

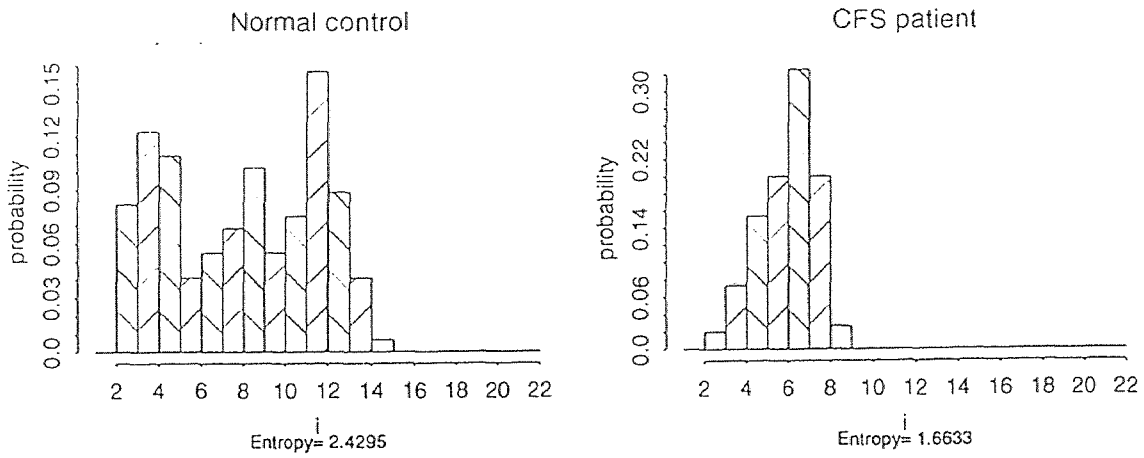

Figure 4.7 Histogram of the probability distribution of the data for suject1 and 10.

The overall entropy was calculated from Figure 4.7 by using (3-10). The value for the normal subject is 2.43 while the value for the CFS subject is 1.66. The results for all subjects are shown in table 4.2.

C. Partial entropy

The partial entropy is used to quantify the dispersion of partial data points spreading on the Y-axis at a certain x-value. We divide the phase space plot into 10×10 boxes as shown in Figure 4.8. and count the points in each box.

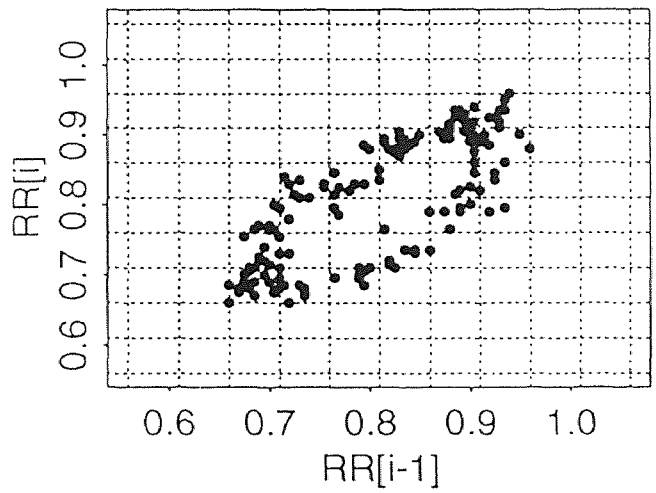

Figure 4.8 Phase space plot divided into 10×10 boxes.

Table 4.2 Individual overall entropy (* normal subject and # CFS patient)

Subject	Stage1	Stage2	Stage3	Stage4	Stage5	Stage6
1*	2.3182	1.7845	1.9305	2.5308	1.5907	1.4624
2*	2.4295	2.0334	1.9899	2.1583	1.8016	1.3951
3*	2.7628	2.7557	2.5416	2.3785	2.3493	1.6713
4*	2.3891	2.2695	1.8389	2.2600	1.9335	1.8873
5*	1.9398	1.4615	0.7730	1.5951	1.0067	0.9302
6*	2.3739	2.1856	2.0323	2.0363	1.6132	1.2362
7*	2.5783	2.3529	2.1016	2.5849	2.3314	1.9519
8*	2.4943	1.7242	1.2357	2.3163	1.8078	1.2420
9*	1.8463	1.9941	1.8313	1.9212	1.2938	1.4416
10#	1.3177	1.3230	1.5029	1.4937	1.0691	1.4154
11#	1.8520	1.5963	0.8711	1.8894	1.7779	1.9651
12#	2.0182	1.5119	1.4946	1.7557	1.2810	1.0763
13#	2.3046	1.7652	1.1601	2.0495	1.7504	1.3519
14#	1.5238	1.4842	1.7343	1.4867	1.3196	1.3634
15#	1.6633	1.6120	1.2314	1.2996	1.4634	1.1665
16#	1.0179	0.9045	0.6709	0.6392	0.6886	0.4721
17#	1.9634	1.9864	1.7808	1.9331	1.8295	1.7900
18#	1.5530	1.2357	1.0737	1.3766	1.1834	1.0771

Let the number of points in the (i,j)th box be x_{ij} and $x_i(m)$ be the total number of points within the ith interval of the X-axis. The probability of x_{ij} at the ith interval of the X-axis can be calculated as follows:

$$P(x_{ij}) = \frac{x_{ij}}{x_i(m)}$$

where

$$x_i(m) = \sum_{j=1}^{8} x_{ij}$$

Figure 4.9 shows the histograms of the probability distribution at all 10 intervals of the X-axis for subject1 and subject10. This figure shows that the width of the distribution is larger for subject1 (normal)(Figure 4.9 (a)) than for subject10 (CFS)(Figure 4.9(b)) in each interval of the X-axis.

The partial entropy is calculated from Figure 4.9 by using the formula (3-12). The value at each interval of the X-axis is larger for subject1 (normal) than that for subject10 (CFS).

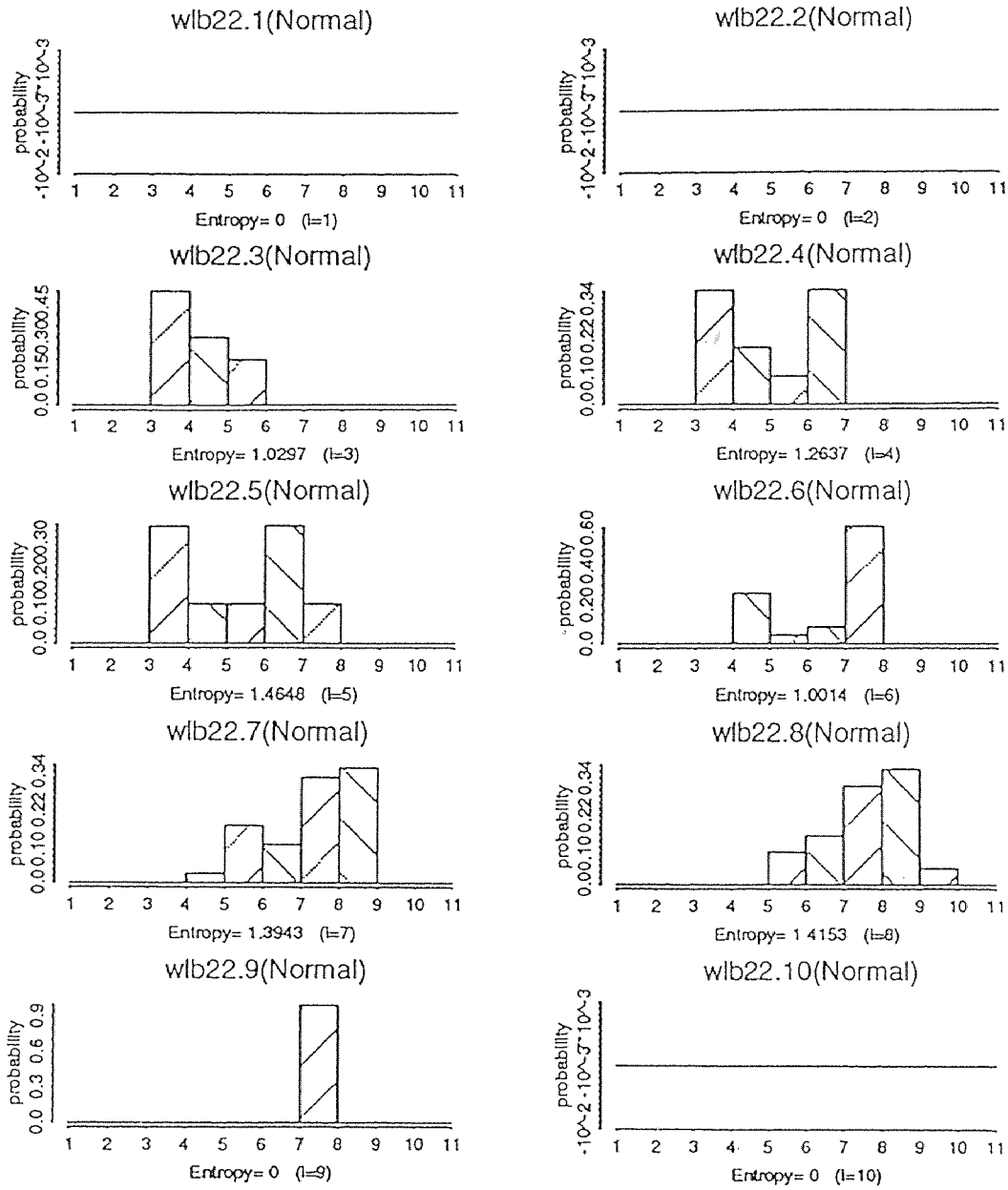

Figure 4.9 (a) Histogram of the probability distribution at 10 intervals of the X-axis for subject1.

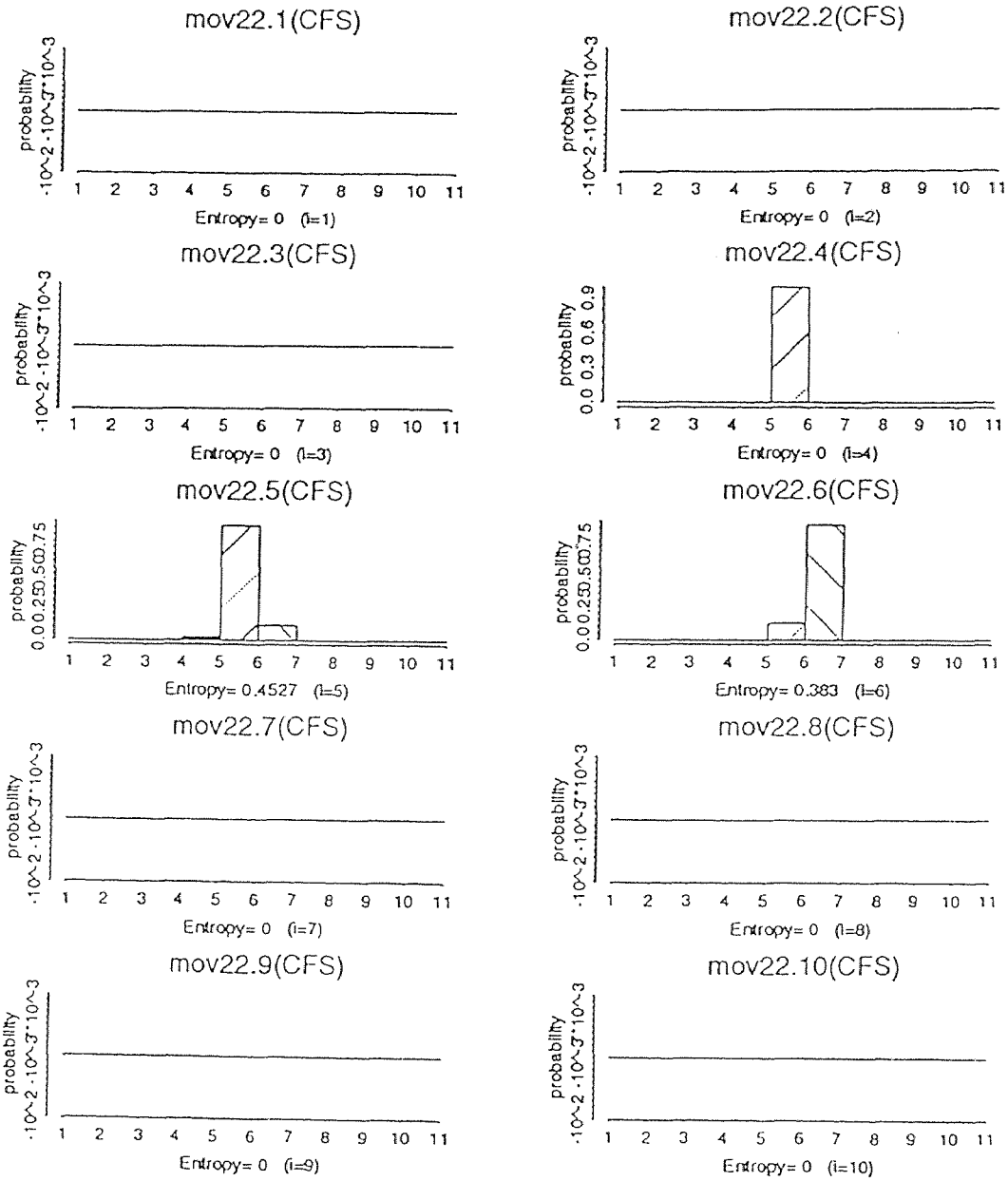

Figure 4.9 (b) Histogram of the probability distribution at 10 intervals of X-axis for subject10.

D. Distribution of probability and overall entropy in different stages

Figure 4.10 shows the histogram of the probability distribution and the overall entropy for all 6 stages for subject1. The left panel shows the result from breathing at 8,12 and 18 cycle/min while sitting. The right side is the result while standing.

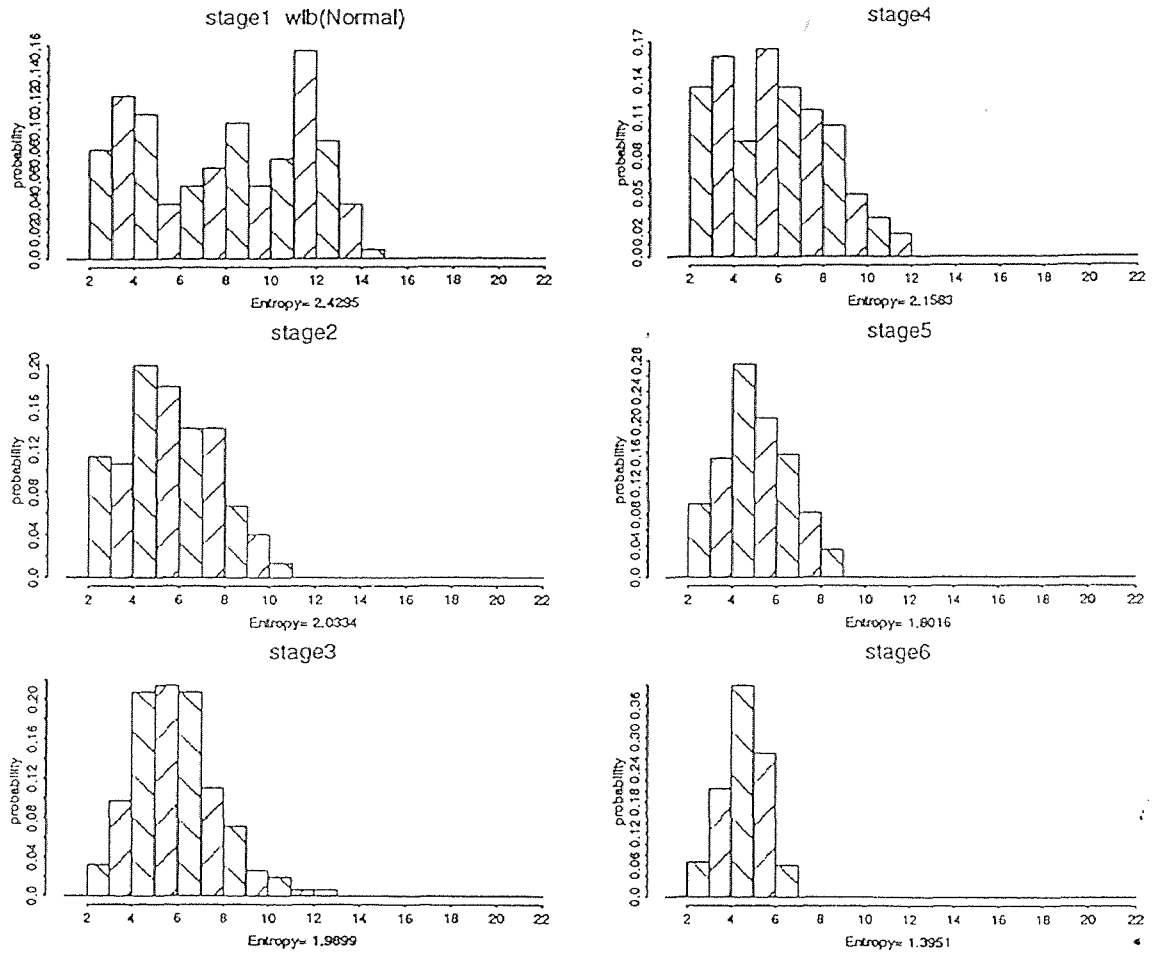

Figure 4.10 Histogram of the probability distribution for six stages for subject1.

With increasing breathing rate, the distribution of probability decreased and the overall entropy dropped from 2.43 to 1.99 while sitting and from 2.16 to 1.40

while standing. Figure 4.10 also shows that the posture affects the width of the distribution. At the same breathing rate the overall entropy while sitting is larger than the value while standing.

E. Result of groups

Figure 4.11 shows the mean value of overall entropy for normal and CFS groups in all 6 stages. The solid line represents the mean value of the normal group and the dotted line represents the CFS group. The normal subjects have larger overall entropy than the CFS patients at each breathing rate. Bars reflects the standard deviation of the data. The results of the two-tailed t-test is shown on the figure as well, which indicates that the difference between these two mean values is significant ($p<0.05$) in every stage. Also, the variation of the curve meets the result described in part D of this section, that is, the overall entropy decreases as the breathing rate increases.

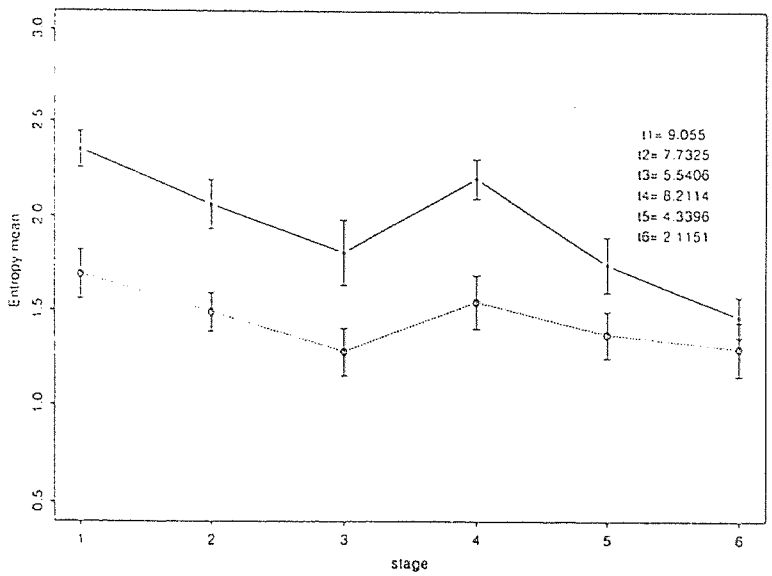

Figure 4.11 Mean of overall entropy in normal and CFS subjects (——— normal,- - - - - - - CFS), stage1,2,3 are breathing at 8,12, and 18 cycle/min while sitting, stage4,5,6 are breathing at 8,12, and 18 cycle/min while standing.

4.3.3 Nonlinear Structure Detection

A. Surrogate data sets

We used the spectral synthesis method (SSM) described in section 3.5 to generate 1000 data sets for each original time series. First we computed the Fourier Transform of the original data and obtained the complex series $A_o=a_o+b_oi$. The amplitude r and phase $\varnothing_o$ are :

$$r = (a_o^2+b_o^2)^{1/2} \qquad \text{and} \quad \varnothing_o = b_o/a_o$$

We then chose a number between $-\pi$ and π randomly from a uniform distribution and added it to $\varnothing_o$ to produce $\varnothing$. Using the same r value and new $\varnothing$ we form a new complex series:

$$A = a + bi$$

where $a = r\cos\varnothing$ and $b = r\sin\varnothing$. We then computed the inverse Fourier Transform of A and obtained a new time series, called the surrogate data set. This new time series has the same power spectrum as the original data set but different phase from the original one. Fig 4.12 shows a time series(IBI signal) and eight surrogate data sets generated by the SSM algorithm. It is not obvious by eye which is the actual data set and which are the surrogates. In this case it is the fifth time series from the top which is the real one.

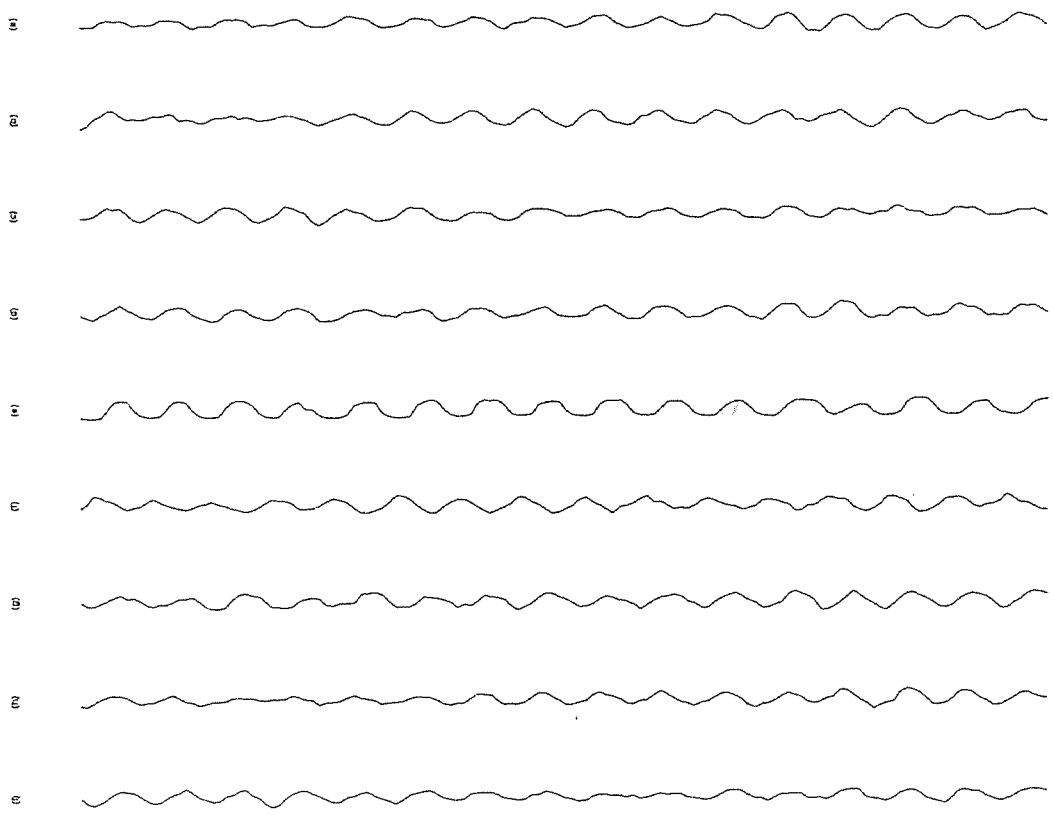

Figure 4.12 Results of nonlinear structure test for each data sets.

B. Computing the correlation dimension and significance

We generated 1000 surrogate data sets for each real data set from stage1 (8 breaths/min while sitting) which included 9 normal subjects and 9 CFS patients and calculated the mean correlation dimension, and standard deviation for each surrogate data set. The results are shown in Table4.3. D_o is the correlation dimension for the original data. D_s is the mean value of the correlation dimension for the 1000 surrogate data sets. Sd (σ_s) is the standard deviation of the surrogate data sets. The S value is calculated by (3-13) which is $S=|D_o-D_s|/\sigma_s$. The first nine subjects are normal people and the others are CFS patients.

Table 4.3 Results of nonlinear structure test for each data set (* normal subject and # CFS patient).

Subject	D_o	D_s	S_d	S	p
1*	2.6883	4.4821	0.5545	3.235	<0.05
2*	2.1407	3.9179	0.4256	4.1757	<0.05
3*	2.4911	3.2499	0.4675	1.6232	>0.05
4*	2.5107	3.2505	0.2683	2.757	>0.05
5*	1.9368	3.4189	0.313	0.313	>0.05
6*	2.0237	3.3825	0.3164	4.295	<0.05
7*	3.0641	3.3449	0.3595	0.7811	>0.05
8*	2.4071	3.329	0.4268	2.1598	>0.05
9*	3.1092	3.1036	0.2631	0.0214	>0.05
10#	2.4283	2.762	0.3529	0.9458	>0.05
11#	2.8464	3.0193	0.4347	0.3978	>0.05
12#	2.8066	3.0116	0.4978	0.4118	>0.05
13#	2.9063	3.1803	0.3728	0.7349	>0.05
14#	2.6078	3.2384	0.5022	1.5577	>0.05
15#	2.9479	3.1847	0.3594	0.5839	>0.05
16#	2.6216	3.3467	0.2744	2.6423	>0.05
17#	2.4996	3.1721	0.2917	2.306	>0.05
18#	2.4836	3.2101	0.3888	1.8685	>0.05

Table 4.3 shows that subjects 1,2, and 6 have significantly different correlation dimensions between the real data and surrogate data ($p<0.05$) which means that the linear hypothesis is rejected and nonlinear structure is detected in these three time series. The test failed for the other data sets.

CHAPTER 5

DISCUSSION AND CONCLUSION

5.1 High Correlation Dimension in CFS Patients

The major finding of our correlation dimension study was the increase of correlation dimension in CFS patients. Analysis of correlation dimension and t tests of grouped data showed that CFS patients had significantly higher correlation dimension than controls at 8 ($p<0.05$), 12($p<0.05$), and 18 ($p<0.01$) breaths per minute while sitting and at 8 ($p<0.01$) and 12 ($p<0.01$) while standing . There was no significant difference between the two groups at 18 breaths per minute while standing.

We have discussed in section 2.3 that the fractal process in heart rate variability was studied as a possible indicator of the complexity of the heart dynamic system and the correlation dimension (fractal dimension) of heartbeat intervals measures the degree of correlation of the heart rate, or reflects the degree of heart rate variability. Our observation showed that there is a higher correlation of heart rate in CFS patients than in normal people. Therefore, the variability of heart rate in CFS patients was reduced which is associated with a loss of physiological complexity.

It is clear that heart rate fluctuations are mainly due to autonomic nervous system control. Any variation of the heartbeat must reflect variation of the nervous system. Therefore, the high correlation dimension or the loss of heart rate variability may represent one or more aspects of autonomic nervous system imbalance. This inference is in agreement with another study on vagal power which used the same data as ours. That study showed that there was a significant difference in vagal power between CFS

5.2 Low Entropy in CFS Patients

The phase space plots described in section 3.4 are simple to construct and are useful tools for assessing two aspects of the dynamics of heart rate. The placement of the scatter within the Y vs. X axes demonstrate the overall range of interval values. In addition, the phase space plot shows the instantaneous variation from one beat to the next (the spread of Y-values at a given X-value).

The phase space plots from controls had similar characteristic shapes (see Figure 4.5). They were characterized by a high beat-to-beat variation (wide spread of Y-values at a given X-value) and a high overall range (large placement of the scatter). The plots of CFS patients had opposite characteristic shapes: narrow spread of Y-values at a given X-value to form a positive diagonal scatter of points and small dispersion.

The entropy of the overall range of intervals E_o quantified the width of the probability distribution of all points along the X-axis. The value of entropy from controls was significantly larger than the value for CFS subjects at 8 ($p<0.01$) , 12 ($p<0.01$) and 18 ($p<0.01$) breathes per minute while sitting and at 8 ($p<0.01$) and 12 ($p<0.01$) while standing. There was no significant difference between the two groups at 18 breaths per minute while standing.

These findings also indicated that the loss of heart rate variability in CFS patients may result from similar physiological mechanisms as those responsible for correlation dimension changes.

In addition, the entropy of data for a given x-value (a given length of interval or heart rate) E_p from CFS patients was significant less than that of controls at every heart rate. These values measured instantaneous changes in beat-to-beat relationship and showed the variability at both high heart rate (short R-R intervals) and low heart rate (long R-R intervals) was significantly reduced in CFS patients.

It is reported that the parasympathetic nervous system directly mediates short-term heart rate variations. Thus, decreased vagal tone may contribute to the reduced beat-to-beat variation. Furthermore, increased sympathetic activation can reduce short-term heart rate variability by inhibiting vagal activation of the heart[26]. Thus, either sympathetic hyperactivity or parasympathetic hypoactivity, or some interaction of the two, may underlie the reduced beat-to-beat heart rate variation. In CFS patients, there was a sustained low variation from low to high heart rate suggesting that CFS patients may suffer from both increased sympathetic tone and impaired vagal tone.

5.3 Reduction of Variation of D_c and E_o with Respiratory Rate

Another significant finding is that the variation of correlation dimension D_c and overall entropy E_o with respiratory rate is reduced in CFS subjects. We have observed that the correlation dimension D_c changed when the respiratory rate changed for both CFS and healthy subjects. So did entropy E_o (see Figure 4.4 and Figure 4.11). But the variation of D_c and E_o with respiration in CFS patients was much less than in controls. From stage4 (8 breaths/min while standing) to stage5 (12 breaths/min while standing), the mean value D_c of controls increased from 2.4482 to 2.7426 (+12%) while the value for CFS patients increased from 2.767 to 2.9328 (+6%). The mean value E_o for controls decreased from 2.1979 to 1.7476 (-20.5%) while the value of CFS patients decreased from 1.547 to 1.3736 (-11%). From stage5 (12 breaths/min while standing) to stage6 (18 breaths/min while standing), the mean value D_c of controls increased from 2.7426 to 3.24 (+18%) while the value for CFS patients increased from 2.9328 to 3.28 (+11%). The mean value E_o for controls decreased from 1.7476 to 1.4687 (-16%) while the value for CFS patients decreased from 1.3736 to 1.2975 (-5.5%).

It is well known that heart rate varies with respiration because the respiration is

associated with periodic discharge of afferent fibers in the lung, activating the parasympathetic nervous system, producing brief perturbations of the cardiac pacemaker which regulates the heart rate. Modulation of cardiac rate by respiration is respiratory-rate dependent. The reduction of heart rate variability in response to respiration infers that the interaction between heartbeat and respiration was changed and the responsivity of the cardiac variability control mechanism to changes of respiratory rate was weakened. This result implied that the autonomic nervous system may be in disorder. In CFS patients, when the respiratory rate changed, the nervous system acts too slowly to affect such rapid adjustments while normal behavior often requires rapid response of the cardiovascular system to physiological demands.

5.4 Reduction of Heart Rate Variability with Increase of Respiratory Rate

Figure 4.4 and Figure 4.11 show that as the respiratory rate increases the correlation dimension D_c increases and entropy E_o decreases. Both of these results indicate that reduction of heart rate variability is associated with higher respiratory rate.

We can suggest from this observation that reduction of heart rate variability may imply the decreased parasympathetic nervous activity because the parasympathetic nervous system contributes to regulate the respiratory rate, with reduced vagal tone (reduced variability) related to higher respiratory rate. The CFS patients who have less heart rate variability may suffer from an infirm parasympathetic nervous system.

From the results of correlation dimension and entropy measurement we speculate that autonomic disturbance may lead to cardiac instability. A primary effect of CFS is a loss of responsivity of cardiac variability control mechanics to physiological needs which is obviously maladaptive for adequate cardiac function. The major effect of CFS is to fix heartbeat interval variation within narrow limits. Although it is not clear that cardiac

instability is a factor in CFS, the changes in dynamic pattern of heart rate reported here indicated pronounced alterations in nervous system control of the heart in the CFS patients.

5.5 Nonlinear Structure Detection

The method of surrogate data is a statistical approach for identifying nonlinearity in time series. We used it to detect possible nonlinearities in the heartbeat interval signals in both normal and CFS subjects. The results (Table 4.3) showed that nonlinearity was detected in 3 time series ($p<0.05$) and not in the others.

There are three possibilities for the test failing to find nonlinear structure: (1) the time series which was detected is a linear stochastic system. This seems incorrect because the IBI signal is a fractal time series which should be nonlinear except for some pathological condition. (2) the data size may be too small to be detected for nonlinearity. (3) the method may need to be modified. Because the phases of the surrogate data are randomized they end up "beating" against each other and producing spurious low-frequency effects. Also spurious high-frequencies can be introduced because there is a jump-discontinuity from the last to the first point during the Fourier transform. Therefore the surrogate data may not keep the same power spectrum as the original one and cause the test to fail.

We considered the latter two possibilities as the most probable cause of failure of the test. To solve these problems, we can use the Amplitude Adjusted Fourier Transform and Window Fourier Transform algorithms. They can modify the surrogate data greatly[9].

5.6 Future Work

The nonlinear techniques we discussed provide a noninvasive method to measure physiologically significant aspects of heart rate variability and have the potential to be useful for diagnosis. Our study has shown that dimension and entropy can distinguish between sick and healthy people, with CFS patients having higher correlation dimension and entropy than healthy ones.

In spite of the apparent association between high correlation dimension D_c, low entropy E_o and CFS patients, we can only speculate on the physiologic basis of the observed association between these two values and CFS. The possible role of correlation dimension and entropy as diagnostic tools has not been addressed. The small sample size of the present study limits any conclusion regarding possible contributions of clinical variables to the outcome. Further investigation will be required. It must be determined whether correlation dimension and entropy are direct prospective indicators of CFS. Future work includes the following:

(1) to collect and analyze more data to verify the conclusions of the present study.

(2) to investigate the dependence of the relationship between correlation dimension, entropy and CFS on different physiological quantities such as respiratory flow, cardiac output, and blood pressure which are regulated by the autonomic nervous system. Knowledge of this dependence will enable us to more fully understand heart rate variability with CFS and its use in diagnosis.

(3) to modify the spectral synthesis method further to detect the nonlinear structure with the Amplitude Adjusted Fourier Transform algorithm and Window Fourier Transform algorithm on large time series. Also we may use other surrogate data generated by shuffling time-order of the original time series to test the nonlinearity of time series.

APPENDIX

PROGRAMS

Calculation of Correlation Dimension

```
      subroutine corr2 (x,c,l)
      double precision x(l)
      double precision m(16)
      double precision c(16)
      integer l
      b0=2
      e=0.55
      b1=b0**(-15*e)
      b2=b0**(-14*e)
      b3=b0**(-13*e)
      b4=b0**(-12*e)
      b5=b0**(-11*e)
      b6=b0**(-10*e)
      b7=b0**(-9*e)
      b8=b0**(-8*e)
      b9=b0**(-7*e)
      b10=b0**(-6*e)
      b11=b0**(-5*e)
      b12=b0**(-4*e)
      b13=b0**(-3*e)
      b14=b0**(-2*e)
      b15=b0**(-1*e)
      b16=b0**(+0*e)
      do 5 i=1,16
      m(i)=0
5     continue
      j=8
      do 40 p=1,l-j
      do 50 n=p+1,l-j+1
      y=0
      do 60 mi=0,j-1
      y=y+(x(p+mi)-x(n+mi))**2
60    continue
      z=sqrt(y)
      if(z.lt.b1) then
      m(1)=m(1)+1
      endif
```

```
if(z.lt.b2) then
m(2)=m(2)+1
endif
if(z.lt.b3) then
m(3)=m(3)+1
endif
if(z.lt.b4) then
m(4)=m(4)+1
endif
if(z.lt.b5) then
m(5)=m(5)+1
endif
if(z.lt.b6) then
m(6)=m(6)+1
endif
if(z.lt.b7) then
m(7)=m(7)+1
endif
if(z.lt.b8) then
m(8)=m(8)+1
endif
if(z.lt.b9) then
m(9)=m(9)+1
endif
if(z.lt.b10) then
m(10)=m(10)+1
endif
if(z.lt.b11) then
m(11)=m(11)+1
endif
if(z.lt.b12) then
m(12)=m(12)+1
endif
if(z.lt.b13) then
m(13)=m(13)+1
endif
if(z.lt.b14) then
m(14)=m(14)+1
endif
if(z.lt.b15) then
m(15)=m(15)+1
endif
if(z.lt.b16) then
m(16)=m(16)+1
```

```
      endif
50    continue
40    continue
      do 100 i=1,16
      if(m(i).ne.0) then
      d=m(i)
      c(i)=alog(d)
      else
      c(i)=0
      endif
100   continue
      do 30 i=1,16
      if(c(i).eq.0) then
      do 70 p=i+1,16
      if(c(i).gt.c(p)) then
      c(i)=c(p)
      endif
70    continue
      endif
30    continue
      return
      end


      m_0.55
      d1_-15*m
      d2_-14*m
      d3_-13*m
      d4_-12*m
      d5_-11*m
      d6_-10*m
      d7_-9*m
      d8_-8*m
      d9_-7*m
      d10_-6*m
      d11_-5*m
      d12_-4*m
      d13_-3*m
      d14_-2*m
      d15_-1*m
      d16_-0*m
      z_c(d1,d2,d3,d4,d5,d6,d7,d8,d9,d10,d11,d12,d13,d14,d15,d16)
      par(mfrow=c(4,2))
      x_scan("wlb.7")
```

```
x_x[1:135]
x_x/200
y_corr2(x)
wlb.6_y[1:16]
a_wlb.6
plot(z,a,xlab=" ",ylab="ln cd")
for(i in 1:9){
if (a[i]<=0) next
a1_i-1
break
}
for (i in 4:16) {
if (a[i]<0.75*max(a)) next
a2_i
break
}
b_lsfit(z[a1:a2],a[a1:a2])$coef
lines(z[a1:a2],b[1]+z[a1:a2]*b[2])
wlb5.s1_round(b[2],4)
title("wlb(Normal)",paste("slope=",wlb5.s1))
```

Calculation of Entropy

```
x1_scan("wlb.2")
z_len(x1)
y_x1
y1_y[1:z-1]
y2_y[2:z]
x_array(0,c(2,z-1))
a_0
b_0
b1_0
h_0
h1_0
d_0
d1_0
e_0
e1_0
f_0
f1_0
g_0
g1_0
i_0
i1_0
```

```
l_0
l1_0
m_0
m1_0
n_0
n1_0
bb_0
bb1_0
hh_0
hh1_0
dd_0
dd1_0
ee_0
ee1_0
ff_0
ff1_0
w_mean(x1)-50
z_z-1
for (j in 1:z){
x[,j]_c(x1[j],x1[j+1])
}
t_10
for (j in 1:z){
if(x[1,j]<w ) a[j]_x[2,j]
if(x[1,j]>=w && x[1,j]<w+t ) b[j]_x[2,j]
if(x[1,j]>=w+t && x[1,j]<w+2*t ) b1[j]_x[2,j]
if(x[1,j]>=w+2*t && x[1,j]<w+3*t ) h[j]_x[2,j]
if(x[1,j]>=w+3*t && x[1,j]<w+4*t ) h1[j]_x[2,j]
if(x[1,j]>=w+4*t && x[1,j]<w+5*t ) d[j]_x[2,j]
if(x[1,j]>=w+5*t && x[1,j]<w+6*t ) d1[j]_x[2,j]
if(x[1,j]>=w+6*t && x[1,j]<w+7*t )  e[j]_x[2,j]
if(x[1,j]>=w+7*t && x[1,j]<w+8*t ) e1[j]_x[2,j]
if(x[1,j]>=w+8*t && x[1,j]<w+9*t ) f[j]_x[2,j]
if(x[1,j]>=w+9*t && x[1,j]<w+10*t ) f1[j]_x[2,j]
}
 for (j in 1:len(b)){
 if (is.na(b[j])) next
if(b[j]>=w && b[j]<w+t ) bb_bb+1
if(b[j]>=w+t && b[j]<w+2*t ) bb1_bb1+1
if(b[j]>=w+2*t && b[j]<w+3*t ) hh_hh+1
if(b[j]>=w+3*t && b[j]<w+4*t ) hh1_hh1+1
if(b[j]>=w+4*t && b[j]<w+5*t ) dd_dd+1
if(b[j]>=w+5*t && b[j]<w+6*t ) dd1_dd1+1
if(b[j]>=w+6*t && b[j]<w+7*t )  ee_ee+1
```

```
if(b[j]>=w+7*t && b[j]<w+8*t ) ee1_ee1+1
if(b[j]>=w+8*t && b[j]<w+9*t ) ff_ff+1
if(b[j]>=w+9*t && b[j]<w+10*t ) ff1_ff1+1
}
k_c(bb,bb1,hh,hh1,dd,dd1,ee,ee1,ff,ff1)
z_bb+bb1+hh+hh1+dd+dd1+ee+ee1+ff+ff1
wlb22.1_k/z
en_0
 for (j in 1:10) {
 if (is.na(wlb22.1[j])) wlb22.1[j]_0
 if (wlb22.1[j]!=0)  en_en+wlb22.1[j]*log(wlb22.1[j])
 }
 if (is.na(en)) en_0 else en_-en
 wlb22.1e_round(en,4)
par(mfrow=c(5,2),mar=c(5,15,5,15))
barplot(wlb22.1,angle=c(45,135),lab=c(10,15,10),histo=T,
        ylab='probability')
 title(" wlb22.1(CFS)",paste("Entropy=",wlb22.1e,"  (i=1)"))
```

Generating Surrogate Data

```
y_scan("wlb.8")
m1_2
m2_7
p_1000
l_len(y)
l0_l/2
ll_ceiling(l0)
if(ll>l0)  l2_l
if(ll<=l0) l2_l-1
x_y[1:l2]
x1_fft(x,inverse=F)
a_atan(Im(x1)/Re(x1))
l3_l2-1
l4_l3/2
#par(mfrow=c(1,2))
b_array(0,c(p,l2))
d_array(0,c(p,16))
for(j in 1:p) {
a1_runif(l4,-3.14,3.14)
l5_l4+2
a11_a[l5:l2]+a1
a22_-rev(a11)
a2_c(a22,a11)
```

```
a3_sqrt(Re(x1)^2+Im(x1)^2)
a4_a3[2:l2]*cos(a2)
a5_a3[2:l2]*sin(a2)
x2_c(x1[1],complex(l3,null,a4,a5))
x22_fft(x2,inverse=T)
x3_x22/l2
b[j,]_round(Re(x3),0)
d11_b[j,]
d22_corr(d11)
d[j,]_d22[1:16]
aa_d[j,]
x4_fft(x3,inverse=F)
x5_fft(x1,inverse=T)
x22_sqrt(Re(x4)^2+Im(x4)^2)
g[j]_slop(aa,m1,m2)
}
wlb.b_b
rm(b)
wlb.d_d
rm(d)
gg_sort(g)
wlb.g_round(gg,4)
write(wlb.g,"wlb.cd",ncol=12)
```

REFERENCES

1. Goldberger, Ary L., David R. Rigney, and Bruce J. West. 1990. "Chaos and Fractals In Human Physiology." *Scientific American.* 262: 42-49.

2. Akselrod, S., David Gordon, Jeffrey B. Madwed, Nancy C. Snidman, Danied C. Shannon, and Richard J. Cohen. 1985. "Hemodynamic regulation: investigation by spectral analysis." *American Physiological Society.* H: 867-875.

3. Shin, Shaw-Jyh, Walter N. Tapp, Stanley S. Reisman, and Benjamin H. Natelson. 1989. "Assessment of Autonomic Regulation of heart Rate Variability by the Method of Complex Demodulation." *IEEE Transactions on Biomedical Engineering.* 36: 274-282.

4. Martin, Gary J., M. Magid, Glenn Myers, Phillip S. Barnett, John W. Schaud, Jerry S. Weiss, Michael Lesch, and Donald H. Singer. 1987. "Herat Rate Variability and Sudden Death Secondary to Coronary Artery Disease During Ambulatory Electrocardiographic Monitoring." *The American Journal of Cardiology.* 60: 86-89.

5. Zhang, P. Z., Stanley S. Reisman, and Walter N. Tapp. 1992. "Heart Rate Variability Study Using Phase Response Curve." *14th IEEE Conference of Biomedical Engineering.* 2: 571-572.

6. Goldberger, Ary L. and David R. Rigney. 1992. "Nonlinear Dynamics, Sudden Death, and Clinical Cardiology." *An NIH Workshop.* June: 27-29.

7. Farmer, J. D. 1982. "Chaotic Attractors of an Infinite-Dimensional Dynamical System." *Physica D.* 4: 366-370.

8. Kaplan, J. D. 1991. "Chaotic Statistics of Biomedical Time Series." *17th IEEE northeast Conference of Biomedical Engineering.* Proceeding: 33-34.

9. Theiler, J., S. Eubank, A. Longtin, B. Galdrikian, and J. D. Farmer. 1991. "Test for nonlinearity in time series: the method of surrogate data." *Proceedings of IUTAM Symposium and NATO Advanced Research Workshop on Interpretation of Time Series or nlinear Mechanical System.*

10. CDS and CFS Research group. 1992. "Chronic Fatigue Syndrome Research at the Cencers for Disease Control." *The CFIDS Chronicle.* Sept.: 50-58.

11. Mandelbrot, B. B. 1982. The Fractal Geometry of Nature. New York. Freeman.

12. Nelson, T.R., B. J. West, and A. L. Goldberger. 1990. "The fractal lung: universal and species-related scaling patterns." *Experientia.* 46: 251-254.

13. Goldberger, A. L. 1992. "Fractal Mechanisms in the Electrophysiology of the heart." *IEEE Engineering in Medicine and Biology.* June: 47-52.

14. Berenfeld, O. 1989. "Simulation of the ventricular depolarization process using a three dimensional heart model with a self-similar conductions system." *Master's Thesis.* Tel Aviv University.

15. Goldberger, A. L. 1987. "Fractals in Physiology and Medicine." *Yale J. Bio Med.* 60: 421- 435.

16. Deering, William and Bruce J. West. 1992. "Fractal Physiology." *IEEE Engineering in Medicine and Biology.* June: 40-46.

17. Mandelbrot, B. B. 1977. Fractals: Form, Chance, and Dimension. W. H. Freeman.

18. Hentschel, H. G. E. and I. Procaccia. 1983. "The infiniter of Generalized Dimensions of Fractals and Strange Attractors." *Physica* 8D: 435-444.

19. Grassberger, P. and I. Procaccia. 1983. "Characterization of Strange Attractors." *Physical Review Letter.* 50: 346-349.

20. Takens, F. 1981. "Detecting strange attractors in fluid turbulence." *Dynamical Syatems and Turbulence.* 898: 366-381.

21. Kaplan, D. T., Mark I. Furman, Steven M. Pincus, Sheila M. Ryan, Lewis A. Lipsitz, and Ary L. Goldberger. 1991. "Aging and the complexity of Cardiovascular dynamics." *Biophysical Journal.* 59: 945-949.

22. Takens, F. 1985. "On the numerical determination of the dimension of an attractor." *Bifurcations. Lecture Notes in Mathematics.* 1125: 99-106.

23. Levy, M. N., H. DeGeest, and H. Zieske. 1966. "Effects of respiratory center activity on the heart." *Circ. Res.* 18:67-78.

24. Sisto, Sue Ann, Walter Tapp, Susan Drastal, Michael Bergen, and Benjamin Natelson. 1993. "Vagal tone is reduced during paced breathing in patients with the Chronic Fatigue Syndrome." To be published.

25. Nakamura, Yoshio, Yoshiharu Yamamoto, and Isao Muraoka. 1993. "Autonomic control of heart rate during physical exercise and fractal dimension of heart rate variability." *The American Physiological Society.* 875-881.

26. Schechtman, V. L., S. L. Raetz, R. K. Harper, A. Garfinkel, A. J. Wilson, D. P. Southall, and R. M. Harper. (1993). "Dynamic Analysis of Cardiac R-R Intervals in Normal Infants and Infants Who Subsequently Succumbed to the Sudden Infant Death Syndrome." *Pediatric Research.* In press.